Surface-layer wind shear and momentum transport from clear-sky to cloudy weather regimes over land

A.M. Koning[1], L. Nuijens[1], F.C. Bosveld[2], A.P. Siebesma[1,2], P.A. van Dorp[3], H.J.J. Jonker[1,3]

[1]Delft University of Technology
[2]Dutch Royal Meteorological Insitute (KNMI)
[3]Whiffle, Delft, The Netherlands
[1]Delft, The Netherlands
[2]De Bilt, The Netherlands
[3]Delft, The Netherlands

Key Points:

- wind
- momentum flux
- cloud regimes
- convection

Corresponding author: Mariska Koning, A.M.Koning@tudelft.nl

Abstract

This study investigates how wind shear and momentum fluxes in the surface- and boundary layer vary across wind and cloud regimes. We use a nine-year-long data set from the Cabauw tower of the Ruisdael Observatory (NL) complemented by (8.2 x 8.2 km^2) daily LES hindcasts. An automated algorithm classifies observed and simulated days into different cloud regimes: 1) clear-sky days, 2) days with convective clouds (cumulus) rooted in the surface layer, with three ranges of cloud cover, and 3) days with clouds not rooted near the surface. Categorized days in observations and LES do not fully match, with a tendency of the LES to develop convective clouds on clear-sky days and less frequently produce non-rooted clouds, whose scales are far larger than the LES domain. Even so, the climatology and diurnal cycle of winds are for each regime very similar in LES and observations, strengthening our confidence in LES' skill to reproduce certain clouds for an atmospheric state. Wind shear is smallest in clear-sky and cumulus regimes with limited cloud cover (CLCC), which also have the weakest 200 m wind speed and largest surface buoyancy flux. They have notably larger cross-wind fluxes, although along-wind momentum flux profiles are similar across all regimes. Cloudy days have larger momentum fluxes distributed over deeper layers, sustaining up to 20% of the surface flux value at cloud base. Compared to clear-sky, the CLCC regimes have stronger updrafts and deeper mixed-layers. At similar atmospheric stability, surface friction is larger and underestimated by Monin-Obukhov Similarity Theory.

Plain Language Summary

Accurate modelling of surface wind speeds is required to improve wind energy prediction and representation of surface fluxes in models, as they influence a range of atmospheric processes. This paper compares the surface layer wind gradients and turbulent momentum fluxes among various wind- and cloud regimes. We use observed and modelled climatological wind and cloud records over the Netherlands, which we grouped into 1) clear-sky days, 2) (cumulus) clouds that interact with the layer below, with three ranges of cloud cover, and 3) all other clouds. We have confidence in the modeled winds and clouds: when comparing the regime-averaged behaviour of wind, temperature, and humidity, the model and observations show similar results. When comparing the different cloud regimes, we find smaller wind speed gradients (difference between wind speed at different altitudes) on clear-sky and shallow cumulus days. Shallow cumulus regimes appear to have larger surface friction than clear-sky regimes when correcting for atmospheric stability.

1 Introduction

Accurate predictions of wind speed and wind direction near the surface are important, for instance to estimate energy generation in wind farms or to predict surface stress, heat and moisture fluxes that influence a range of atmospheric processes. The short-term local wind forecast relies on many processes, of which several are not resolved in numerical weather prediction (NWP) models but parameterized. Unresolved parameterized processes that impact the winds are surface drag and shear-driven turbulence, as well as convection and gravity waves. Over land the deepening of the boundary layer due to turbulence and dry convection is typically accompanied by the development of shallow cumulus clouds. The objective of this study is to investigate the relationship between wind shear and momentum fluxes with cloud or weather regimes and identify whether convective cloud regimes in particular, as opposed to clear sky regimes, have a different structure of wind and momentum flux near the surface.

There are a number of ways through which winds and clouds relate. First of all, clouds are inherently coupled to certain wind or weather regimes. For instance, in the Netherlands, cloudy days typically have westerly winds bringing moist air masses onto

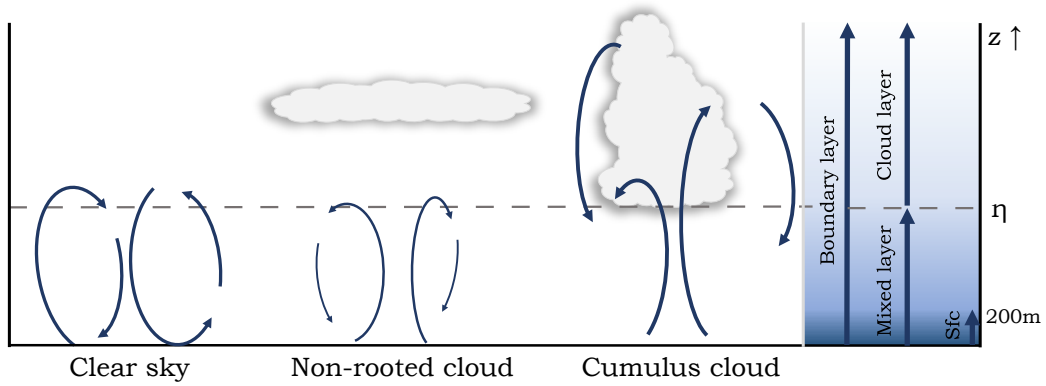

Figure 1. The main cloud regimes and associated boundary-layer scale circulations are shown. Stratus layers may obstruct a large part of the solar radiation, reducing the updraft strength. Thicker arrows correspond to stronger up- and downdrafts. The dashed horizontal line indicates the top of the mixed-layer (η). On the right, we specify the definitions of the boundary layer (for the cumulus regime), mixed-layer, cloud layer and surface layer (indicated as "Sfc" and taken as the layer up to 200 m). In the cumulus cloud regime, the mixed-layer is identical to the sub-cloud layer, whereas in the clear-sky and non-rooted cloud regime the mixed-layer comprises the entire boundary layer.

land, whereas days with easterly winds and high surface pressure tend to be associated with clear skies. Significant (deep) convective and stratiform cloudiness are associated with the passage of storm systems coming from the west, while congestus clouds prevail after cold-front passages and in cold air outbreaks from the north.

Second, as illustrated in Figure 1, clouds alter the surface energy budget through radiation, which influences turbulence and convection in the boundary layer. He et al. (2013) contrasted entirely cloud-free days (clear skies) over the Netherlands with days that have persistent low level cloudiness (cloud base height <1.5 km, at least 10 cloud base detections out of a maximum of 20 detections per 10 min) and found that winds in the surface layer are less well-mixed (have larger shear) on cloudy days, because of reduced incoming solar radiation at the surface and reduced surface buoyancy fluxes.

Third, shallow cumulus clouds are naturally rooted within the surface layer and develop as a results of thermal circulations driven by the surface buoyancy flux (that may already be larger than on clear sky days). The turbulent mixing that drives clouds will also drive different winds. Detecting the convective plumes using wavelet analysis, Schalkwijk et al. (2010) exposed the thermal structure in the boundary layer up to 200 m (in observations), as well as the full boundary layer (in LES). They found that thermals are responsible for 40% of the total vertical heat transport. Thermals can however also violate the often used Monin-Obukhov Similarity Theory (MOST) to estimate fluxes in the surface layer. Fodor et al. (2019) found that convective scale up and downdrafts may not have locally determined properties and may produce deviations from MOST estimated buoyancy flux in the limit of free convection cite. Even when MOST still holds, Li and Bou-Zeid (2011) found that momentum transport in the near surface layer (<10 m) became less efficient when the atmosphere became more unstable, opposed to buoyancy. They explained the lower efficiency by the increased importance of transport through convective plumes rather than through small-scale turbulent eddies.

Fourth, convective clouds may deepen the boundary layer and lead to deeper vertical mixing of scalars and wind (Stevens, 2007). Clouds may also alter turbulent circulations through mesoscale organization (Bretherton & Blossey, 2017; Holloway et al., 2017) or through evaporatively-driven downdrafts, for instance, the gustiness associated with density currents driven by evaporation of rain (Jabouille et al., 1996, e.g.). Early flight campaigns showed that organization may change the turbulent momentum flux. (LeMone & Pennell, 1976) measured in three convective situations over the ocean near Puerto Rico: on a suppressed day with almost no clouds, a day with shallow roll convection, and a day with enhanced shallow popcorn convection and numerous clouds. The two days with suppressed convective conditions had down-gradient diffusive fluxes that act to reduce the wind shear, whereas the case with enhanced convection showed significant counter-gradient transport, especially below and near the bases of clouds, something that is typically associated with organized systems of deep convection (LeMone, 1983; Rotunno et al., 1988; LeMone & Jorgensen, 1990; Wu & Yanai, 1994; Tung & Yanai, 2002). Convective cloud organization is currently an important topic in studies of trade-wind convection, where mesoscale variability in cloud, rain, wind and scalars is pronounced (Stevens et al., 2017).

Over land such studies are rarer (Moeng & Sullivan, 1994; Zhang & Klein, 2013; Van Stratum et al., 2014) and the relationship between near-surface wind and convective or boundary layer tops is not well described. Much of what we know about momentum transport by shallow convection in fact stems from Large Eddy Simulation of cumulus convection over the ocean (ATEX, BOMEX, RICO) (Brown, 1999; Schlemmer et al., 2017; Zhu, 2015; Saggiorato et al., 2020). Even for the ocean, such cases are highly idealized, with constant large-scale (wind) forcing and domains too small to allow for convective organization. Zhu (2015) exemplified just how different the simulated turbulent flux profiles are and can even change sign depending on cloud regime and the scales of the transport e.g., small-scale shear-driven eddies or larger coherent circulations. This motivates studying momentum flux profiles for a wider variety of cases and conditions as present in real nature.

In our study, we use a long climatology (2009 – 2016) of cloud and wind measurements collected at Cabauw (now part of the Ruisdael observatory (`https://ruisdael-observatory.nl/`)) to study how near-surface wind and momentum flux change with cloud regimes. Measurements by a ceilometer and 200 m tall measurement tower are complemented by small-domain (8.2 x 8.2 km^2) LES runs of the same long period. The LES output provides insight into the turbulence processes, such as the momentum flux profiles, extending beyond 200 m. By distinguishing days with clouds that are rooted in the surface layer (which we label convective clouds) from days with clouds that are not rooted and days without clouds, our analysis aims to answer how wind shear in the surface layer changes in the presence of different cloud regimes, and whether convective cloud regimes are accompanied by different wind mixing behavior than clear sky or overcast regimes after accounting for differences in surface buoyancy fluxes, atmospheric stability and large scale wind.

In the next section, we will describe the measurements taken at Cabauw, the set-up of the LES and the selection method for the different cloud regimes. The cloud regimes as identified in the observations and in the LES will be verified and compared. In the results we first describe the differences in wind mixing and momentum flux in the surface layer, using data from both observations and LES. Second, we will discuss differences for the entire boundary layer, for which only LES results are used. Conclusions are presented in section 4.

2 Data

2.1 Cabauw (Ruisdael) observational data

The observational data contain 10-minute interval measurements of wind speed and direction taken at the tower using cup anemometers and wind vanes. The anemometers and wind vanes are mounted on 10 m long booms that are positioned at 40, 80, 140 and 200 m height. Because wind measurements are sensitive to flow obstructions, only the undisturbed measurements are selected from the three booms that measure wind direction and from two booms measuring wind speed. Winds at 10 and 20 m are measured at three different masts (70 m and 140 m NE, 30m SE from the main mast) to avoid flow disturbance by main mast itself and the small buildings attached to the main mast. The selection of these separate masts depends on the wind direction. Momentum fluxes are estimated from wind measurements of sonic anemometers located at 5, 60, 100 and 180 m height, and are available every 10 minutes. They are corrected for streamline tilt due to flow obstruction around the masts and by instruments. Low frequency losses are corrected for according to Bosveld (1999). Further details can be found in Bosveld (2020)

Cloud base height (cbh) is measured by a LD40 ceilometer. The LD40 is situated on a field to the south of the tower, within 50 m from the mast, which justifies synergistic use of the data (Bosveld et al., 2020). On this field, also the net radiation and net surface fluxes are measured. The ceilometer measures back-scatter intensity from particles using a 855 nm wavelength. The maximum range (detection height) is 13600 m with a resolution of 7.5 m. It emits 65000 pulses every 15 seconds, and returns three cloud base heights, as well as vertical visibility and a precipitation index. We only use the first (lowest) measured cloud base, because the signal attenuates considerably after penetrating a cloud. Furthermore, we disregard any back-scatter retrievals from altitudes above 5 km, as convective clouds have cloud bases below 5 km and we assume that clouds above 5 km do not have an influence on the mixed layer other than through radiation. The first detected cloud base height is not necessarily the height that corresponds to the lifting condensation level, where one expects convective clouds to have their base. It can correspond to cloud edges, sides of slanted clouds, or stratiform outflow. In section 3, we describe in more detail how we use this information to classify cumulus days. Note that we make a clear distinction between cloud cover and cloud fraction. We refer to cloud cover as the areal fraction of the sky that is covered with cloud, which is measured by the ceilometer and can be calculated from the LES output. We use cloud fraction only to refer to the amount of cloud at any height; such profiles are only available from the LES.

2.2 Large Eddy Simulations

LES models solve the filtered Navier-Stokes equation at fine resolution. Although LES was traditionally used to study turbulence in the boundary layer, it has proven to be adequate for simulating convective, cloudy boundary layers. Our LES data is generated with the commercially-used GPU-Resident Atmospheric Simulation Platform (GRASP), whose first version was based on the Dutch Atmospheric Large Eddy Simulation (DALES). For more information on DALES we recommend reading (Heus et al., 2010). GRASP has been modified to run on Graphics Processing Units (GPUs) instead of Central Processing Units (CPUs), increasing the computational speed considerably, making it suitable for operational use in the wind energy industry. In our case, GRASP is run in hindcast mode, obtaining its daily initial and large-scale forcing conditions from ECWMF's (European Centre for Medium-Range Weather Forecast) ERA5 data. This forcing includes the radiative heating profiles, which means that the surface energy budget does not "feel" the clouds resolved by LES, but those produced by the Integrated Forcasting System (IFS). We will see later that this does not lead to a major difference as compared to the observations. For more information on the coupling to ERA5, please see

Schalkwijk et al. (2015). To enable the long period of daily hindcasts computational burden is limited by using a relatively small domain, which is 8.192 km^2 by 5.079 km with a horizontal resolution of 64 m and a vertical resolution that decreases with height from 16 m near the surface to 80 m at approximately 5 km. In the model, the sub-grid scheme of Sullivan et al. (1994) is used. Additionally, a heterogeneous surface model is applied to every gridbox individually, following TESSEL (ECMWF, 2015), using high resolution land use data from the CORINE (`https://land.copernicus.eu/pan-european/corine-land-cover`) data-set. Apart from ensuring a correct local surface roughness, the heterogeneous surface conditions ensure a sensible roughness experienced by the in-flowing wind. This roughness is similar to the average roughness in the domain due to periodic boundary conditions, which is reasonable as the region around the domain are quite similar to the conditions at Cabauw.

Each run is initialised at 21:00 UTC and runs to 23:59 UTC the next day. To avoid spin-up influences and overlap in the data, we use the output data from mid-night to mid-night. Data output consists of domain and hourly averaged profiles, including profiles that are conditionally sampled on updraughts ($w > 0$), cloudy updraughts ($w > 0, q_l > 0$), cloud ($q_l > 0$) and cloud-core ($w > 0, q_l > 0, \theta'_v > 0$). Furthermore, profiles of wind, temperature, and humidity are output for the exact location of the Cabauw tower and liquid water path (LWP) snapshots are given every 10 minutes for the full horizontal scale of the domain, from which cloud cover is estimated.

3 Cloud regime classification

We identify three different cloud (weather) regimes:

1. Clear-sky (dry convective boundary layer)
2. Convective clouds rooted in the sub-cloud layer
3. Other clouds not rooted in the sub-cloud layer

The dry convective regime may be associated with convection in a boundary layer whose top lies below the lifting condensation level. The second cloud regime corresponds to clouds on days where the lifting condensation level is reached by convection, and cumulus clouds form. The third regime may be any cloud that does not have a base close to the lifting condensation level e.g., altostratus or cirrus.

Typically, cumulus clouds form before noon and disappear around 12:00 – 13:00 UTC (season dependent). Therefore, we frequently contrast regimes for the hours between 10:00 – 16:00 UTC, which contains the local mean solar time noon at 11:40 UTC. During those times, the buoyancy flux should be positive, and cloud bases should lie near the LCL. Of course, not all cumulus clouds are shallow cumulus. Also stratocumulus and deep convective clouds have a base close to the LCL, yet those cloud types are associated with larger cloud cover. Therefore, we further separate the cumulus regimes by the cloud cover into three sub-regimes: 5 - 30%, 30 - 70% and 70-100%.

Assigning days to the above cloud regimes has to be done differently in the observational data than in the LES data. Both are described next.

3.1 Selecting cloud regimes in observations

To classify each day into a cloud regime, we will use: a) the average surface buoyancy flux during daytime hours, i.e. 10:00 – 16:00 UTC (12:00 –18:00 local summer time, 11:00 –17:00 local winter time, b) the temporal cloud cover (CC) during 10:00 – 16:00 UTC, derived from the number of ceilometer profiles with a detected cloud base; c) the distribution of first detected cloud base heights with respect to d) the lifting condensation level (LCL), converting Bolton's formula for temperature at LCL (Bolton, 1980) to

Table 1. Sensitivity cloud regime selection for different thresholds for distance to LCL (D_{LCL}) and fraction of cbh detections near LCL (f_{LCL}).

	Fraction of cbh detection near LCL: $f_{LCL} = 30\%$			Tolerance distance: $D_{LCL} = 200m$	
	$D_{LCL} = 100m$	$D_{LCL} = 150m$	$D_{LCL} = 200m$	$f_{LCL} = 50\%$	$f_{LCL} = 70\%$
Obs					
Clear-sky	316 (10.0%)	316 (10.0%)	316 (10.0%)	316 (10.0%)	316 (10.0%)
CC 5-30%	167 (5.3%)	187 (5.9%)	199 (6.3%)	170 (5.4%)	130 (4.1%)
CC 30-70%	236 (7.5%)	351 (11.1%)	421 (13.4%)	218 (6.9%)	106 (3.3%)
CC >70%	356 (11.3%)	508 (16.1%)	643 (20.4%)	363 (11.5%)	239 (7.6%)
Other	2073 (65.9%)	1786 (56.7%)	1569 (49.8%)	2081 (66.1%)	2357 (74.9%)

a height from each temperature, relative humidity and specific humidity measurement at the tower at 200 m altitude during 10:00 – 16:00 UTC (Romps, 2017).

The following criteria apply for each of the cloud regimes:

1. Clear-sky: Average surface buoyancy flux is positive, cloud cover is <5%.
2. Convective clouds: Average surface buoyancy flux is positive, cloud cover is $\geq 5\%$, $> 30\%$ of cloud base heights are located at the LCL $\pm$ 200 m. We further separate by cloud cover: CC $= 5-30\%$ ("shallow cumulus"), CC $= 30-70\%$ ("congestus and deep convection") and CC $= 70 - 100\%$ ("stratocumulus and deep convection").
3. Other clouds: All remaining days, including days with negative surface buoyancy fluxes or days with $< 30\%$ of cloud base heights at the LCL $\pm$ 200 m.

The 30% cloud base height threshold is subjectively chosen and evaluated. It is motivated by the fact that in previous studies of shallow convection (albeit in the trades) approximately 2/3 of the detected cloud bases are near LCL, whereas the other third are from cloud edges, sides of slanted clouds, stratiform outflow, etc. (Nuijens et al., 2014). Because cloud fields over the Netherlands are more diverse, we require only a third of the cloud bases to be near the LCL.

We tested the sensitivity of the selection to different thresholds for the number of detected cloud bases near LCL and the distance to LCL. This is presented in Table 1. We compared these statistics with a (manual) visual classification made for the year 2016. For the by-eye classification, we used the ceilometer back-scatter profiles, the cloud webcam and the satellite images of NASA's Moderate Resolution Imaging Spectroradiometer (MODIS) satellites Aqua and Terra (`https://worldview.earthdata.nasa.gov/`). The ceilometer back-scatter profiles provide a good view on the growth of the boundary layer, whether the cloud base grows along with the boundary layer, and whether there are multiple cloud layers and different cloud types present. The cloud camera and satellite visual image gave further insight into the cloud type and the general cloud conditions around Cabauw. A confusion matrix of the objective classification with our chosen thresholds against the by-eye selection is shown in Table 6. This table indicates how many days classified by-eye as a certain regime are also classified by the automated algorithm as such. Large values on the diagonal are desired, as this indicates that the algorithm and the by-eye classification agree.

Table 2. Confusion matrix for cloud regime selection in observations in the year 2016. To classify in the rooted cloudy days, the cloud base needed to lie for 30% of the time within 200m from LCL.

		Algorithm					
		Clear sky	CC 5-30%	CC 30-70%	CC > 70 %	Other	Total Visual
Visual	Clear sky	39				4	43
	CC 5-30%	4	33			2	39
	CC 30-70%			31		11	42
	CC > 70%				23	24	47
	Other	1	4	13	48	112	178
	Total alg.	44	37	44	71	153	349

The visual inspection shows that the algorithm does well in selecting the clear-sky days and shallow cumulus days. The more cloud fraction, the more difficulties the selection algorithm has in separating the convective clouds from other cloud types. Especially the overcast cumulus days are hard to separate from other overcast conditions, something to bear in mind when interpreting those results.

3.2 Selecting cloud regimes in LES

To select convective clouds in LES, we use a) the surface buoyancy flux, b) the areal cloud cover, c) the LCL and d) the first height where the cloud fraction maximizes, all determined during daytime hours (10:00 UTC – 16:00 UTC) and averaged over the model domain. The cloud cover is estimated from (10 min averaged) snapshots of the liquid water path. To avoid detecting small excursions from zero as the lowest local cloud fraction maximum, we have set a minimum value of 1% cloud fraction. If no maximum exists (e.g. when there is a domain filling cloud from the top of the domain downward), we use the first height at which the cloud fraction is 1%.

The following criteria apply for each of the cloud regimes:

1. Clear-sky: Average surface buoyancy flux is positive, cloud cover is <5%.
2. Convective clouds: Average surface buoyancy flux is positive, cloud cover is $\geq$ 5%, and at least 4 out of 7 hours have a local maximum in cloud fraction at the LCL $\pm$ 200 m. In addition, the cloud fraction below 200 m should be $\leq$ 1% (no fog). We further separate by cloud cover: CC = 5–30%, CC = 30–70% and CC = 70 – 100%, as in the observations.
3. Other clouds: All remaining days, including days with negative surface buoyancy fluxes, days with < 4/7 hours with a cloud fraction maximum at the LCL $\pm$ 200 m, or days with fog.

The main difference between the selection method in observations and in LES is the criterion to check whether clouds are rooted. LES gives a cloud fraction profile, averaged over the hour, whereas in observations we have data every 10 seconds. Therefore, the hourly cloud fraction in LES is likely to have clouds every hour, leading us to look

Table 3. Sensitivity cloud regime selection for different thresholds for distance to LCL and fraction of cbh detections near LCL.

	Fraction of cbh detection near LCL: $f_{LCL} = 4/7$			Tolerance distance: $D_{LCL} = 200m$	
	$D_{LCL} = 100m$	$D_{LCL} = 150m$	$D_{LCL} = 200m$	$f_{LCL} = 3/7$	$f_{LCL} = 5/7$
LES					
Clear-sky	482 (14.8%)	482 (14.8%)	482 (14.8%)	482 (14.8%)	482 (14.8%)
CC 5–30%	195 (6.0%)	237 (7.3%)	244 (7.5%)	285 (8.8%)	195 (6.0%)
CC 30–70%	518 (15.9%)	562 (17.3%)	567 (17.4%)	583 (17.9%)	835 (16.5%)
CC >70%	799 (24.6%)	833 (25.6%)	835 (25.7%)	852 (26.2%)	807 (24.8%)
Other clouds	1259 (38.7%)	1139 (35.0%)	1125 (34.6%)	1051 (32.3%)	1231 (37.8%)

Table 4. Confusion matrix for the selection based on cbh using the local cloud maximum as cbh in 2016 with a tolerance of 200m and fraction of 4/7 hours. No cloud below 200m also applied.

		Algorithm					
		Clear sky	CC 5-30%	CC 30-70%	CC > 70 %	Other	Total Visual
Visual	Clear sky	63				1	64
	CC 5-30%		27			6	33
	CC 30-70%			52		8	60
	CC > 70%				73	16	89
	Other		2	2	26	89	119
	Total alg.	63	29	54	99	120	365

only at whether (some) cloud is present during the individual hours. To get an idea of the sensitivity, we applied different thresholds. These are summarised in Table 3.

The LES selection is not very sensitive to changing the allowed distance from LCL from 150 m to 200 m. However, from 100 to 150 m there is a large difference in the convective cloud selection. The shallow cumulus regime is most sensitive, whereas the convective regimes with larger cloud covers are least sensitive.

The confusion matrix for the LES comparing the classified days with the visual inspection and manual classification (2016 only), Table 4, indicates better performance than the automated algorithm applied to observations Table 6. Perhaps this is not entirely surprising, as nature might include more variability than the model. Even though LES has better classification of the cloud regimes, it remains most difficult to tell apart overcast cumulus days from other, non-convective clouds.

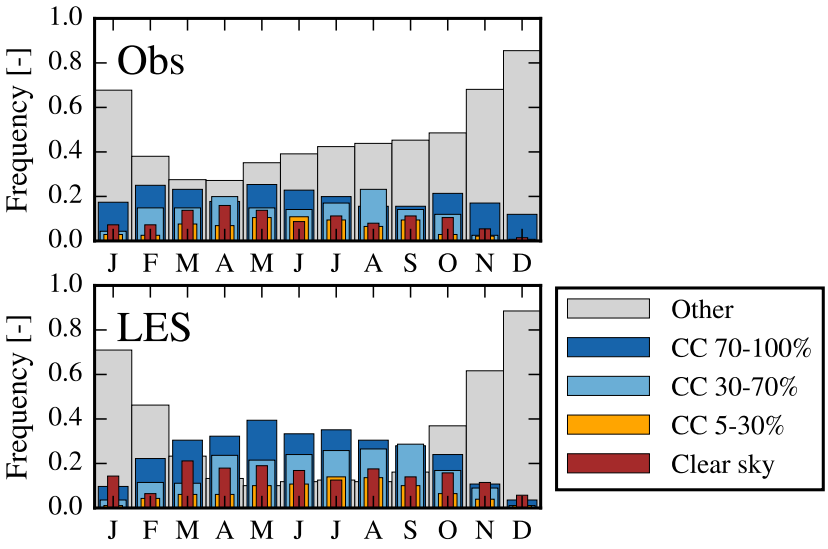

Figure 2. Distribution of the five cloud regimes per month for years 2009–2017. Upper panel: Observations, lower panel: LES.

Table 5. Confusion matrix comparing the cloud regime selection in observations and LES.

		LES					
		Clear sky	CC 5-30%	CC 30-70%	CC > 70 %	Other	Total Obs
Observations	Clear sky	243	27	8	3	31	312
	CC 5-30%	24	88	59	3	24	198
	CC 30-70%	8	59	207	75	71	420
	CC > 70%	1	4	62	309	258	634
	Other	130	64	219	417	723	1553
	Total LES	406	242	555	807	137	3097

3.3 Validating the LES against observations

Intuitively, we expect more overcast days in winter and more clear-sky or fair-weather cumulus days in the spring and summer months. This is reflected in the distribution of the cloud regimes over the different months, whose character is similar in observation and LES (Figure 2). The distribution of days falling into each cloud regime shows low cloud cover cumulus days peak in summer (June, July, August). We also constructed a confusion matrix that compares days classified in LES and observations for the entire climatology. This also reveals an overall good agreement in the relative distribution of days into the different cloud regimes (Table 5). As a turbulence model that lacks a feedback with the large-scale circulation, the LES appears to favor the formation of convection and clouds compared to the observations: more convective days are categorized from the LES at the expense of other, non rooted cloud regimes.

Table 6. Confusion matrix for cloud regime selection in observations in the year 2016. To classify in the rooted cloudy days, the cloud base needed to lie for 30% of the time within 200m from LCL.

		Algorithm					
		Clear sky	CC 5-30%	CC 30-70%	CC > 70 %	Other	Total Visual
Visual	Clear sky	39				4	43
	CC 5-30%	4	33			2	39
	CC 30-70%			31		11	42
	CC > 70%				23	24	47
	Other	1	4	13	48	112	178
	Total alg.	44	37	44	71	153	349

The largest difference between observations and LES is found between convective clouds with CC >70% and the regime with other clouds (Table 1 and 3). We accept this shortcoming, because our interest is majorly on an accurate and thus stricter detection of shallower types of convection, for which we optimized our selection.

In the remainder of our study, we compare statistics within the cloud regimes, which, as these tables indicate, do not necessarily include the exact same days. This is not a concern, because our objective is not to check whether the LES captures daily weather, but instead we are looking to expose the physics that accompany specific cloud regimes. As we will show next, the observations and the LES largely agree on the weather conditions that accompany the different cloud regimes.

4 Climatology of cloud regimes

Figure 3 shows histograms of observed mean temperature, relative humidity (RH), zonal and meridional wind speed (averaged over the lowest 200 m), and surface buoyancy flux during the daytime hours (10:00 – 16:00 UTC) for the five cloud regimes. Typical continental fair-weather (clear-sky days and days with convective clouds but lower cloud cover) is associated with warm and relatively dry surface layers and positive buoyancy fluxes (by definition). This reflects that such regimes are most common in Spring and (early) Summer (Figure 2). The cloudier regimes occur on days with larger RH, which in the case of the non-rooted other cloud regimes is frequently in winter and likely associated with storm passages and negative surface buoyancy fluxes. Cloudy days are generally days with westerly winds, which bring relatively moist air from the ocean on to land, whereas a relatively large portion of the clear sky days happen when winds are from the east. Convective clouds are not restricted to warm fair-weather. The Netherlands experiences regular occurrences of cumulus congestus and even deeper convection on days with cold air outbreaks (typically northwesterly winds) and after frontal passages (typically southwesterly winds). We believe these events are within the intermediate and high cloud-cover regime (in light and dark blue).

Figure 4 shows a similar climatology for the LES, but then in terms of averaged vertical profiles of cloud fraction, thermodynamics and the horizontal wind components extending up to heights of approximately 5 km. To maintain vertical structure, the height axis is scaled by the mixed-layer height (η), defined as the height of the minimum buoy-

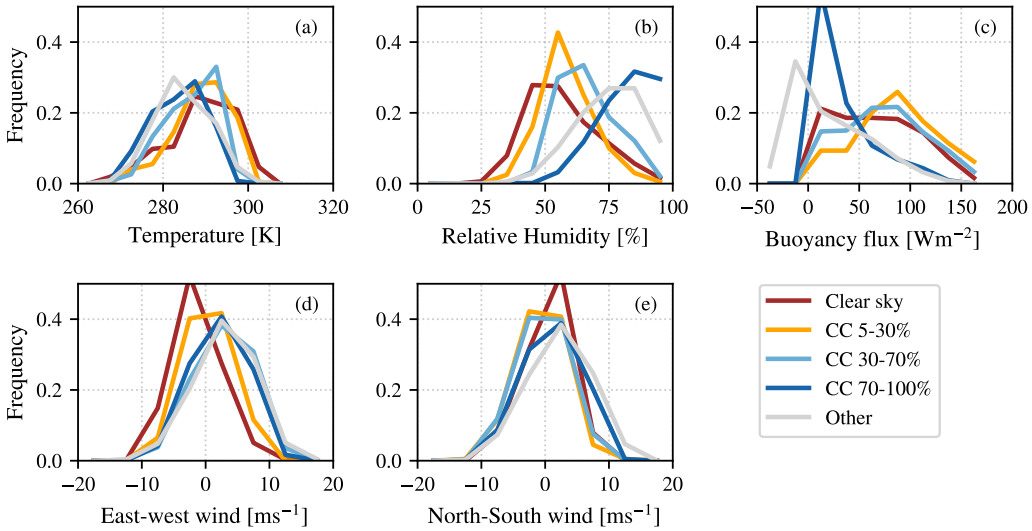

Figure 3. Distribution (histogram) of observed temperature, relative humidity, surface buoyancy flux, zonal wind u and meridional wind v for each cloud regime. Positive zonal winds indicate winds from the west and positive meridional winds indicate winds from the south. Except for the surface buoyancy flux, all variables are averaged over the lowest 200 m and between 10-16 h UTC.

ancy flux and often coinciding with cloud base. The cloud fraction profiles confirm our classification, revealing the classical cumulus cloud fraction profile for the low CC cumulus regimes (yellow and blue lines), whereas the peak below z/η cloud be a signature of stratocumulus days and the peak above z/η could represent days with deeper cumulus (in dark blue). The non-rooted other cloud regime (*e.g.,* westerly storms, in grey) also contains days with fog and other stratus layers. Like the histograms (Figure 3) the clear sky and low CC cumulus days are warm and relatively dry, with weaker westerlies or even easterly winds. Profiles of virtual temperature are well mixed in all cloud regimes. The mixed-layer height is clearly visible in the temperature, relative humidity as well as the wind speed profiles and often coincides with cloud base height.

From a careful observation of the wind profiles we can already notice that the zonal u wind is well mixed in the boundary layer in all regimes, but especially in the clear sky and low to intermediate CC cumulus regimes. In turn, these have a larger wind turning throughout the boundary layer, reflected by larger wind shear (vertical gradients) in the meridional component. In the following, we will look more closely at wind shear in the surface layer and address whether there are notable differences in how winds are vertically mixed depending on the regime.

5 Wind gradients in the surface layer

To address surface layer wind gradients and the degree of wind mixing in the morning and afternoon we adopt the analysis of He et al. (2013) and plot wind speeds at different heights as a diurnal cycle. We do this for both the observations (Figure 5) and the LES (Figure 6). Because the observation heights are not the same as the LES grid heights, we interpolated the LES wind linearly to the observation heights. The general characteristic of the wind diurnal cycle is a larger wind gradient (wind shear) during the night and a smaller wind shear during the day. During the night, the boundary layer be-

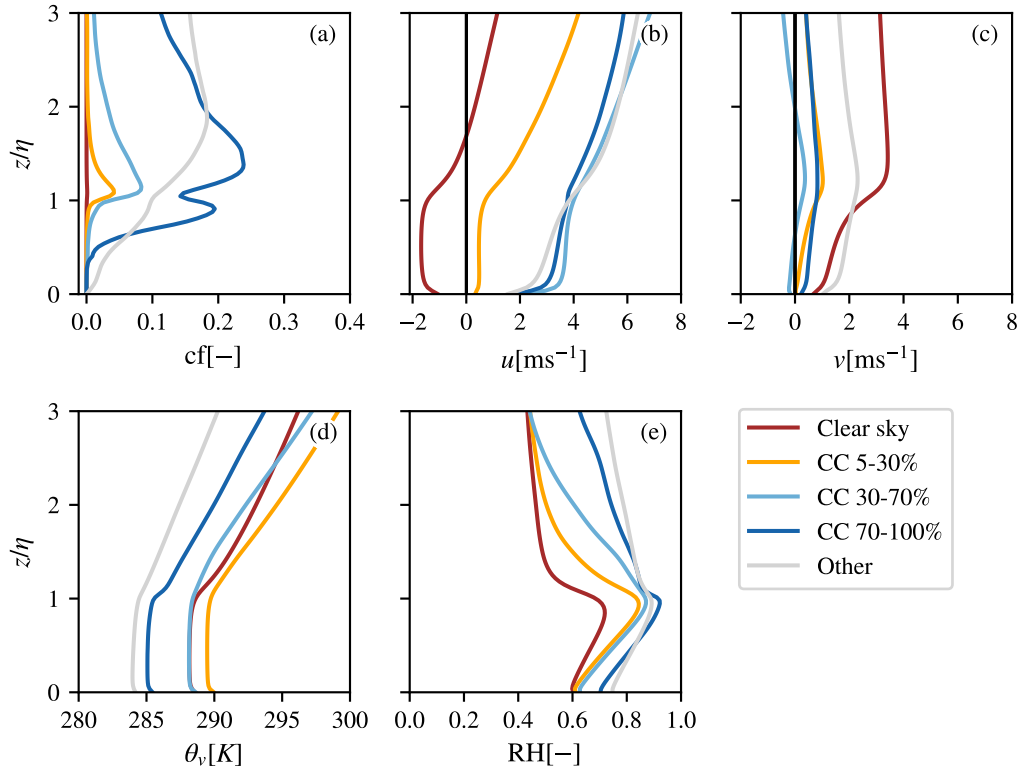

Figure 4. LES cloud regime averaged profiles of (a) the cloud fraction, (b) east-west wind speed (positive eastward) u, (c) south-north wind speed (positive northward) v, (d) θ_v and (e) relative humidity.

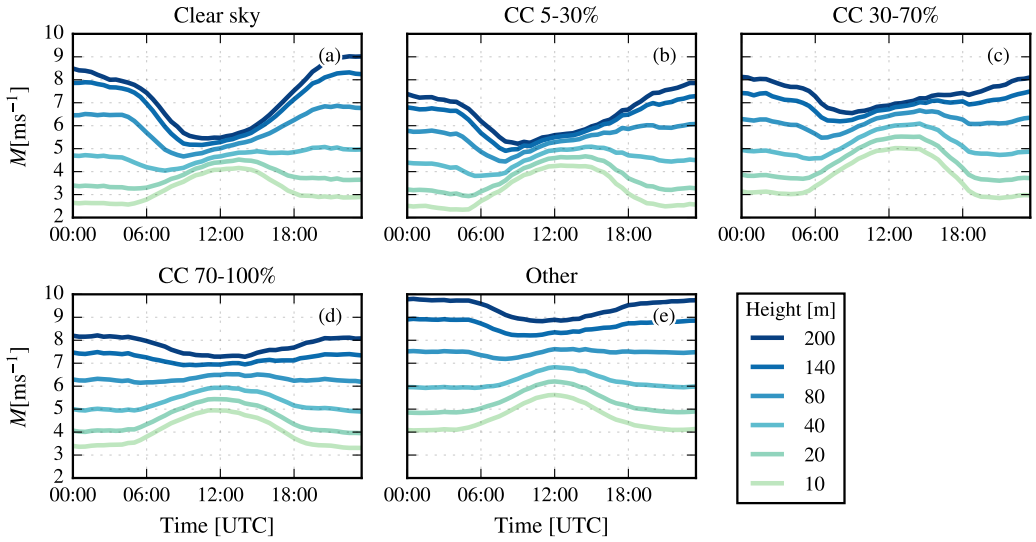

Figure 5. Average diurnal variations of wind speed (M) at five levels of the measurement tower at Cabauw under different cloud regimes. Observations between 2009 and 2017 (incl.) are shown.

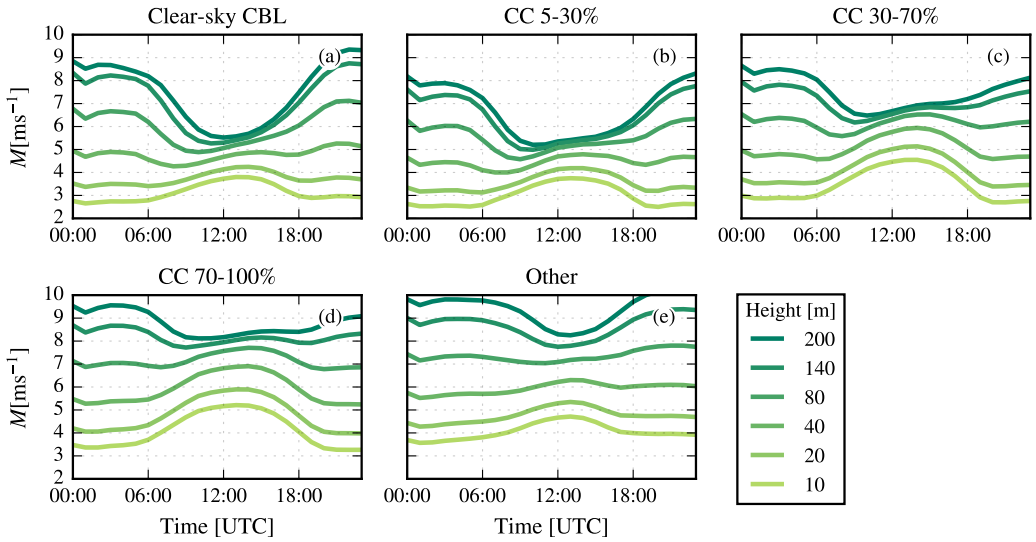

Figure 6. Average diurnal variations of wind speed (M) in LES under different cloud regimes, interpolated to the five levels of the observation tower at Cabauw. Simulations run for 2009 to 2017 (incl.).

comes shallower and stratified, and turbulent mixing is reduced. At Cabauw, the boundary layer height sometimes becomes smaller than the tower enabling us to detect nocturnal low level jets (LLJ). LLJs are measured 20% of the nights, usually between 140 – 260 m above the surface and with wind speeds from 6 – 10 ms^{-1} (Baas et al., 2009). The characteristics of the diurnal cycle per cloud regime are all well-captured by LES (Figure 6). The main difference with the observations is in the wind speed. At night the LES usually has faster winds between 80 – 200 m, whereas during the daytime, observations usually show a stronger mean wind at 10 m. With the exception of the overcast convective cloud regime, the observations and the LES are very similar in the upper surface layer.

During daytime, wind shear is reduced in all regimes, especially between 80 and 200m. The smallest wind shear (strongest mixing) is observed on clear-sky days and days with low cc convective clouds, which are also the days that have the largest surface buoyancy fluxes (Figure 3c). The overcast cumulus and non-rooted cloud regimes, which are associated with lower surface buoyancy fluxes, have larger vertical shear, as expected based on the study by He et al. (2013).

From about 12:00 UTC, when wind shear is generally smallest, wind at all height levels in the surface layer increase with time in the clear-sky and lower CC cumulus regimes. This may be caused by the deepening of the boundary layer, leading to entrainment of higher momentum air from the free atmosphere into the boundary layer. Indeed, the lower CC cumulus regimes are associated with deeper mixed layers, whose tops are identified as the minimum of the surface buoyancy flux (Figure 7). Increases in wind speeds may also be connected to sea breeze effects which have been observed in ∼8.3% of the days from May to August (Arrillaga et al., 2018).

Figure 8 shows that the total momentum flux at 60 m increases during daytime and peaks slightly after noon, when the buoyancy flux is large and when wind shear is smallest. In LES, the total flux is larger for the cloud regimes with larger wind speed at 200 m, but observations show lower flux for the highly cloudy regimes (CC > 70% and other).

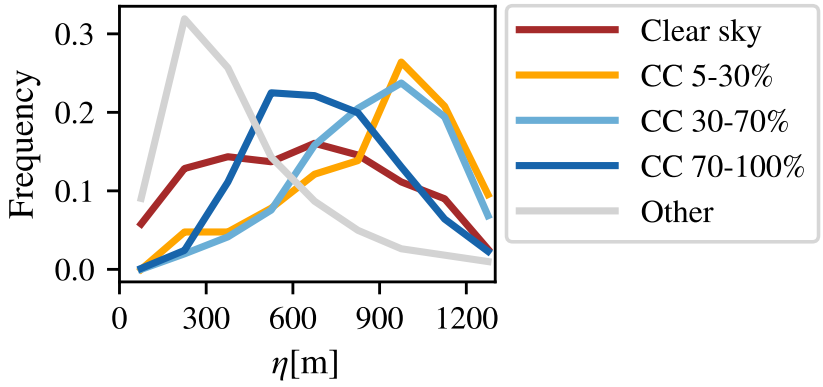

Figure 7. Distribution of the mixed layer top (η) within each cloud regime, from LES.

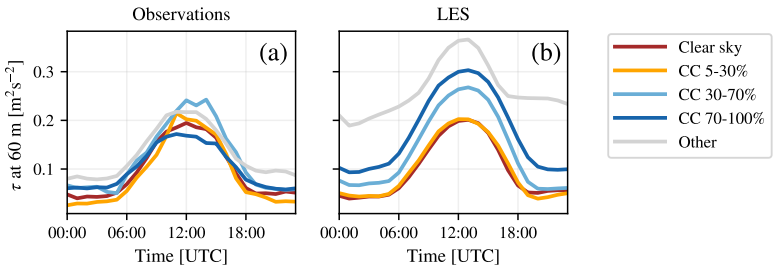

Figure 8. Average diurnal cycle of the total momentum flux (τ) at 60 m for each cloud regime in a) observations and b) LES.

As these highly cloudy regimes have more stable atmospheric conditions, there may be a larger footprint of regional roughness that differs more between the observations and LES than a smaller (local) footprint.

Evidently, the different climatology (weather regimes) associated with the different cloud regimes plays an important role in the degree of wind mixing in the surface layer *e.g.* fair weather cumulus days form on days with larger buoyancy fluxes, weaker stability and weaker large-scale winds. Therefore, wind shear is by definition already smaller. In the following section, we account for the differences in stability and large-scale wind to identify which differences in wind shear across cloud regime remain.

5.1 Non-dimensional wind gradients following Monin-Obukhov Similarity Theory

From the climatology of the cloud regimes, we know that the clear-sky and cumulus regimes deviate from the main climatology: they have weaker winds and a stronger buoyancy flux. This may introduce a very different mixing structure and momentum transport than days with strong wind and weak buoyancy flux (Moeng & Sullivan, 1994). The effect of the surface buoyancy flux and the large-scale wind is illustrated in Figure 9. The wind speed at the surface must go to zero, and therefore, the wind shear is largely determined by the 200 m wind. In Figure 9 we normalise the wind by the daily average wind speed at 200 m and show the composite diurnal cycle for days in three different surface buoyancy flux categories (on the y-axis) and three different 200 m wind categories,

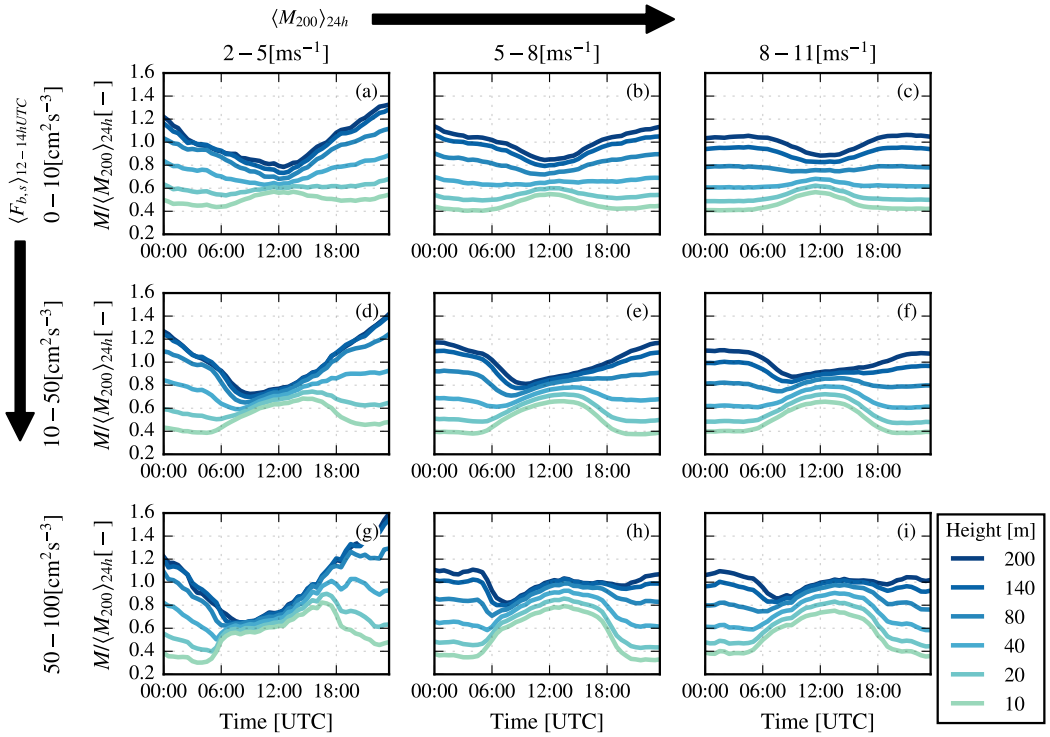

Figure 9. Diurnal cycle of wind speed as observed at the Cabauw tower when the data is separated on 12-14h UTC average surface buoyancy flux and daily average wind speed at 200m.

where we take the 200 m wind as a measure of the strength of the large-scale wind. The stronger the wind (towards the right in each row), the larger the shear. An increase in the surface buoyancy flux also leads to better mixed winds at first, but increasing it beyond 50 $\mathrm{cm^2 s^{-3}}$ does not make a major difference, other than making the winds more variable and causing a stronger increase in wind speed during the afternoon.

To account for the covariability between wind and stability with convection, we use the Obukhov length. The Obukhov length (L), given by:

$$L = -\frac{\overline{\theta_v}}{kg}\frac{u_*^3}{(\overline{w'\theta'_v})_s}, \tag{1}$$

in which θ_v stands for the virtual potential temperature near the surface, u_* for the friction velocity at the surface, k for the von Kármán constant, g for the gravitational acceleration, and $(\overline{w'\theta'_v})_s$ is the surface buoyancy flux. The friction velocity u_*, defined as $u_* = (\overline{u'w'_{sfc}}^2 + \overline{v'w'_{sfc}}^2)^{1/4}$, denotes the turbulent momentum flux at the surface and is thus a measure of momentum destruction in the surface layer. Convective and stable conditions are distinguished by the sign of the buoyancy flux: a negative Obukhov length corresponds to a positive surface buoyancy flux and a more unstable atmosphere. Furthermore, a large negative Obukhov length implies either a small buoyancy flux and / or a large friction velocity, and thus more neutral conditions. Vice versa, a small negative Obukhov length indicates more unstable conditions.

If we contrast the different cloud regimes *at a given Obukhov length*, we may identify whether other processes than stability play a role in setting the surface layer wind shear. Figure 10 (observations) and 11 (LES) show two parameters as function of classes

of stability ($-1/L$), which are all averaged between 12:00 – 14:00 UTC. We only look at an unstable atmosphere ($-1/L > 0$, with weakly unstable (more neutral) conditions on the left and more unstable conditions on the right). Panel a shows the ratio of the 80 m and 200 m wind, as a measure of the wind shear: the closer the ratio to 1, the smaller the shear. Panel b shows the universal similarity function ϕ_M(z/L), commonly known from Monin-Obukhov Similarity Theory (MOST), which is defined as:

$$\phi_M = \frac{\kappa z}{u*} \frac{\partial u}{\partial z}. \tag{2}$$

We approximate ϕ_M from the 12:00 - 14:00 UTC averaged winds and estimate $\partial_z u$ from M80 and M200.

In the observations, across all stability classes, the regimes with convective clouds with cloud covers 5-30 and 30-70% (yellow and light blue) have a relatively larger M_{80} to M_{200} ratio than the clear-sky regime (red), which in turn has a larger ratio than the overcast convective and non-rooted cloudy days (dark blue and grey). We can remove any hidden dependence on u_* when looking at ϕ_M. The general behavior of ϕ_M is to decrease from neutral to unstable conditions as L is reduced (towards the right). The regimes have separate curves, whereby the convective cloud regimes (yellow and light blue) exhibit smaller ϕ_M values than clear skies. In other words, at a given wind gradient these regimes have larger frictional velocity (larger momentum fluxes) near the surface. This suggests that deeper or stronger convective circulations sustain larger 80 m wind speeds compared to a situation where only shear-driven turbulent stresses are present. The vertical bars indicate the standard error and reveal that variability is larger in more unstable classes. These classes also include less samples (days), but it may also reflect that convective scales do not make a large difference when the atmosphere is already unstable.

The LES confirms this picture, although there are notable differences. For instance, values for ϕ_M are overall smaller in LES than for the observations, which is probably because the observed and simulated roughness lengths are different. Cabauw is known to have a complicated land surface, with grassland and small roughness lengths felt close to the surface, and trees and a larger roughness length felt at greater heights. Overcast convective conditions are more similar to the "shallow cumulus" regimes. We do not overinterpret these results, because it is likely that the LES poorly represents the dynamics of deeper cloud regimes on the small domain that is used.

In general, the LES reproduces the different character of the momentum mixing under clear skies and (shallow) convective days, and therefore, we can examine additional statistics from the LES.

We have also plotted the behavior of the mixed-layer height for different stability classes (panel d). The mixed layer depth is typically considered as the characteristic length scale of large convective eddies, and the influence of such large eddies can be taken into account by explicitly including the boundary layer depth in the universal similarity functions (Liu et al., 2019; Fodor et al., 2019).

As we saw earlier in Figure 7, the convective cloud regimes are associated with deeper mixed layers. Next, we will explore wind profiles and momentum flux profiles for the different regimes across the entire boundary layer and not just near the surface.

5.2 Wind and momentum flux profiles

Can we identify difference sin momentum transport between cloud regimes? This is where the LES output is particularly valuable, because it provides momentum fluxes at height levels extending beyond the tower height. Not only the wind speed, but also

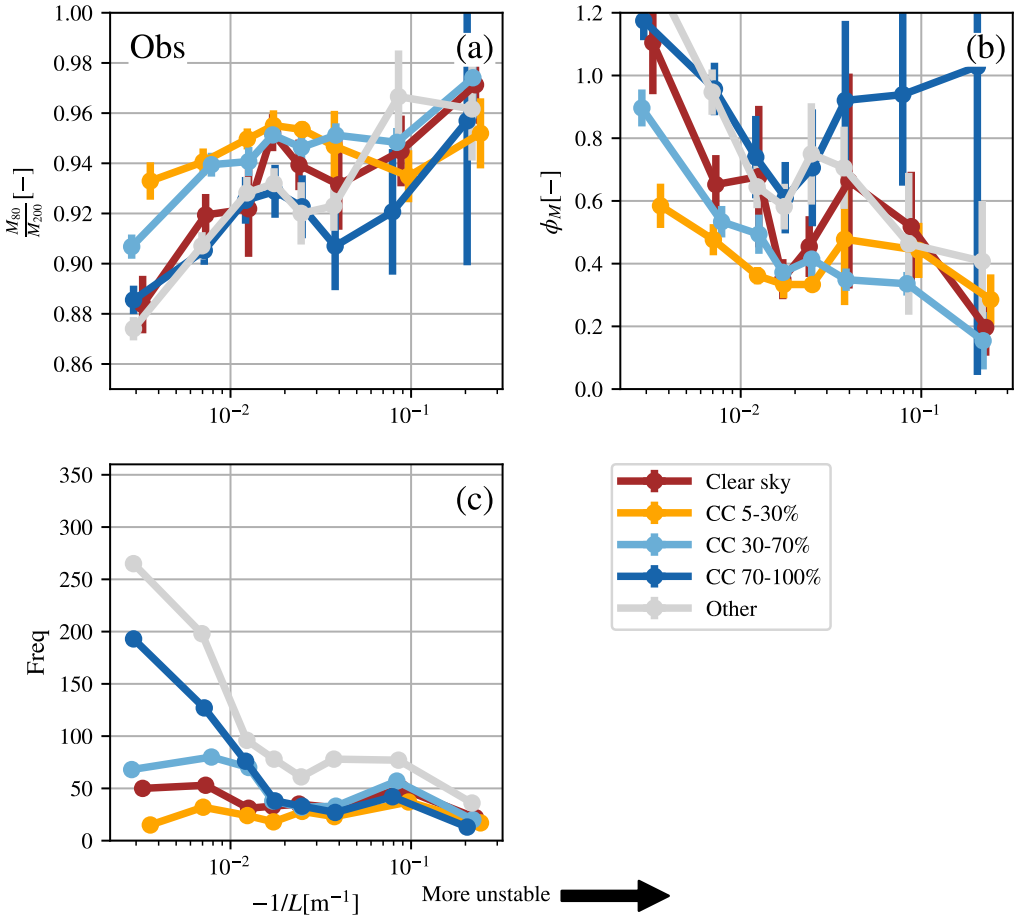

Figure 10. Observations: a) Ratio between the wind speed at 80 and 200 m, b) universal similarity functions, and c) the number of days within each -1/L bin for the five cloudiness categories. Error bars in panel a) and b) indicate the standard error. All data is averaged over the hours 12-14 UTC.

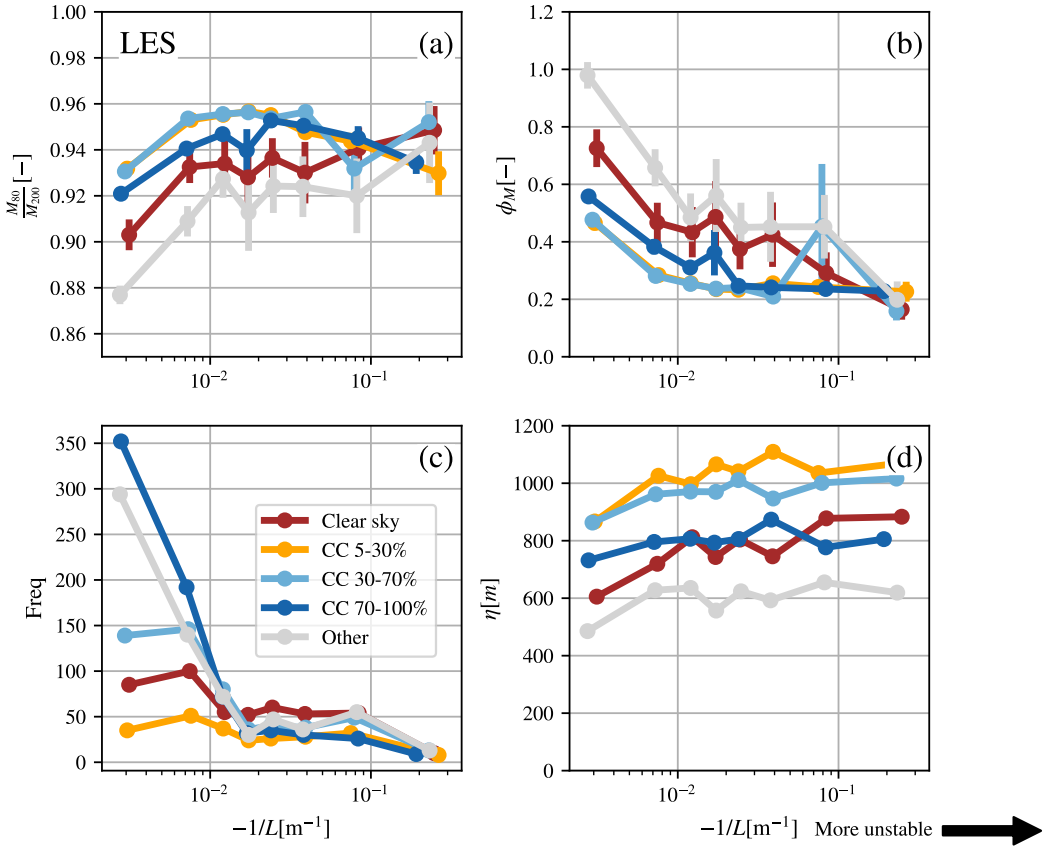

Figure 11. LES: a) Ratio between the wind speed at 80 and 200 m, b) universal similarity functions, c) the number of days within each -1/L bin, and d) average mixed layer height for the five cloudiness categories. Error bars in panel a) and b) indicate the standard error. All data is averaged over the hours 12-14 UTC.

the wind direction varies at Cabauw. For instance, there are regular episodes with easterly winds and westerly winds in the clear sky regime, see Figure 3. Changes in wind directions are associated with a change in sign of the momentum flux, which upon averaging, can bias the momentum flux towards small or zero values. We therefore transform the winds to a natural coordinate system whereby the positive (streamwise) s-axis at every height level points in the direction of the hourly mean of the wind, while the (normal) n-axis is defined perpendicular and anti-clockwise from the positive s-axis. From the along-wind and cross-wind components at each height we calculate the momentum fluxes, which are then normalised by the friction velocity squared and plotted against the non-dimensional height axis z/η. The mean along-wind and cross-wind profiles for each regime are shown in Figure 12 a and b. In essence the cross-wind component tells us how the wind is turning with height in the boundary layer with the wind at the lowest 10% of the mixed layer as a reference. A negative cross-wind implies a (clockwise) veering of the wind with height. The average flux corresponding to a veering or backing cross wind, is similar of shape but has a different sign. The magnitude of the flux differs between backing and veering winds: the slower backing winds have smaller (normalised) fluxes. The general tendency is the same in both cases: in the lower mixed-layer the wind is slowed down, whereas in the upper part the cross wind is typically sped up. As in Figure 4 d and e, days with a large cloud cover and / or no convective clouds (dark blue and grey) are days that tend to have strong westerly winds (*e.g.,* storm passages) and larger wind shear across the mixed-layer. The cross-wind component for $z/\eta < 1$ is small in all regimes, implying a well-mixed sub-cloud layer. Substantial wind turning is pronounced near the mixed-layer height (or cloud base).

The other panels in Figure 12 show the skewness of the vertical velocity (c) and the non-dimensional along- and cross-wind fluxes (d, e), as well as the total momentum flux τ (f). Note that the average of the total momentum flux τ is unequal to the sum of the average along- and cross-wind fluxes as we first calculate τ, normalise it, and then average over each cloud regime. The momentum fluxes clearly reveal how turbulent mixing extends beyond $z/\eta = 1$ for the cloudier categories (light blue to dark blue and grey). For instance, the normalised total momentum flux τ decreases with height approximately linearly (Figure 12 f), but is still at least 30% that of its surface value at $z/\eta = 1$ for the overcast regimes in blue and grey, as well as the "congestus" regime in light blue.

The clear-sky and cumulus regime with low cloud cover have a normalized total momentum flux at $z/\eta = 0.5$ that is close to 1 (Figure 12 f). The relatively large flux is primarily generated in the cross-wind component (Figure 12 e). The strong wind turning or wind jump at the top of the mixed layer can play a role at producing larger shear-driven stresses. Additionally, (convective) eddies can contribute to flux at these levels. These regimes (in blue and yellow) have the largest vertical velocity skewness in the sub-cloud layer (Figure 12 c), indicating stronger updrafts and more coherent plumes may be more effective at transporting slow momentum from the surface towards the mixed-layer top. This is in correspondance with the observational study by Lareau et al. (2018) who found that medium cloud cover cumulus (30-50%) have largest skewness.

In the along-wind component of the momentum flux (12 d), profiles are more similar, but there is less flux below $z/\eta = 0.7$ in the convective regimes with CC $< 70\%$ (yellow/blue). Perhaps, because the wind profiles are already better mixed in these regimes (Figure 12 a), there is less momentum flux generated within the mixed-layer.

The momentum tendency is determined by the negative flux divergence as:

$$\partial_t u_{\parallel}(z) \propto -\partial_z \overline{u'_{\parallel} w'(z)}, \tag{3}$$

where $\partial_t = \frac{\partial}{\partial t}$, and similarly for ∂z. Faster decrease of the flux with height implies that $\partial_t u_{\parallel} < 0$: the wind speed in the direction of the mean flow reduces. The two

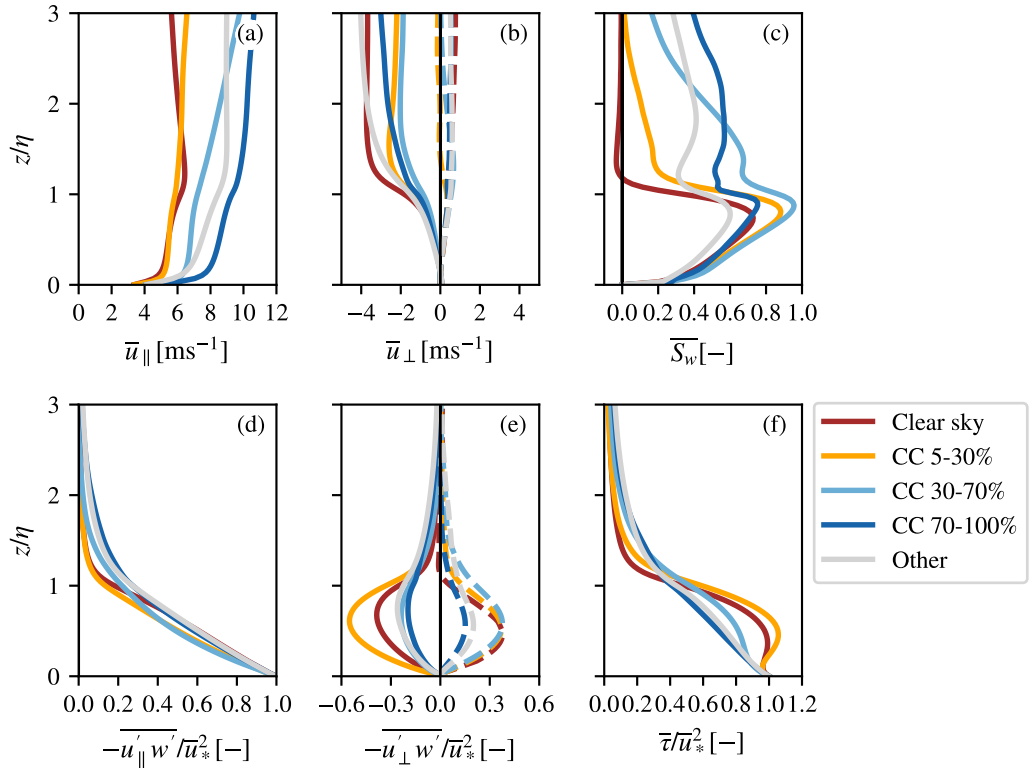

Figure 12. Cloud regime averaged LES profiles of the (a) mean wind, (b) cross wind (c) skewness of vertical wind, momentum fluxes in (d) parallel and (e) cross wind direction , and (f) total flux for the five cloud regimes. Dashed lines in panel (b) and (e) indicate the backing wind cases. All variables are normalised by the mixed-layer height, fluxes are also normalised using the surface friction velocity.

convective cloud regimes thus experience a slightly greater friction throughout the mixed-layer.

6 Conclusion & discussion

This study aims to answer: "Does the surface-layer wind shear and momentum flux profiles change in different cloud regimes ?" In particular, we are motivated by the idea that convective clouds are associated with different momentum transport and winds in the layers below. To explore such statistical relationships, we used a long time record of observations and daily LES hindcasts, which allow us to group different cloud regimes together across a wide range of atmospheric states.

We designed an automated classification that flags a day as belonging to a convective cloud regime based on several criteria, including having a positive surface buoyancy flux during daytime and having a cloud base close to the theoretical LCL. We contrasted these convective days - with three classes of cloud cover - to clear sky days and days with other types of clouds, such as mid or high-level cloud not rooted in the surface or mixed layer. The wind, temperature and humidity climatology and mean diurnal cycle of winds belonging to the different cloud regimes are very similar in LES and observations, even if the classifications do not results in the exact same set of days.

Both LES and observations show that clear-sky days are driest and have easterly winds more frequently. In the convective cloud regimes, relative humidity indeed increases for regimes with larger cloud cover. In LES, cumulus clouds having less than 30% cloud cover are on average warmer. The number of days classified as overcast and "other clouds" differ most between observations and LES. The "other clouds" regime, which we associate with westerly mid-latitude storms from the sea, is the most challenging to simulate because the model is traditionally used for dry convection or shallow moist convection and is ran on a very small domain. Overall, we have confidence in the LES' skill to reproduce clouds for a given atmospheric state, especially clear-sky days and low cloud-cover convective regimes (shallow cumulus and "congestus" days).

We find that clear sky days and convective cloud days have a very similar diurnal cycle of the surface layer wind, with a large wind gradient during nighttime that is mixed away during daytime. Low cloud-cover convective cloud regimes (shallow cumulus) generally have weaker winds and larger buoyancy fluxes than clear-sky and highly cloudy days, and therefore have a head start in mixing away the nighttime wind shear. They also produce a steady increase in mean surface layer winds during the afternoon associated with the development of a deeper boundary layer and presumably the entrainment of higher momentum air. However, we must keep in mind that shallow cumulus days oversample warmer days from late spring to early autumn. Hence, because of the larger insolation in these month, the average buoyancy flux is larger than that of the clear-sky regime that is better distributed over the year.

Evidently, the factors that help form convective clouds in the first place such as large surface buoyancy fluxes also help reduce surface layer wind shear. By further grouping the data into different stability classes defined by the Obukhov length, we attempt to remove the influence of surface buoyancy fluxes and surface friction velocity (set by the large scale wind) on the wind gradients. This reveals that convective cloud regimes have smaller surface-layer wind gradients compared to clear sky days at a similar neutral or weakly unstable stability. We also find that the Monin Obukhov non-dimensional wind gradient function ϕ_m , which relates the surface friction velocity to the surface layer wind gradient, is smaller for the convective cloud regimes with less than 70% cloud cover. This would imply that for a similar wind gradient (large scale wind), more momentum flux is generated on those convective cloud days compared to clear sky or overcast days. It also suggests, as shown by Liu et al. (2019); Fodor et al. (2019), that empirical Monin-Obukhov similarity functions do not explicitly include the effect of large scale up- and downdrafts associated with convective eddies (using the scaling of boundary layer depth) underestimate the momentum flux that is generated in the surface layer.

The non-dimensional momentum flux profiles throughout the entire boundary layer in the direction of the mean near-surface wind are very similar for the different regimes at midday, which suggests that small-scale shear-driven momentum diffusion still dominates the momentum flux. Larger differences are found in the non-dimensional cross-wind momentum fluxes, where the clear-sky and shallow convective clouds regimes have much more momentum flux in the mixed layer. These regimes also have stronger updrafts. Compared to clear sky days and shallow cumulus days, the convective overcast and other cloud regimes have much more cross-wind momentum transport extending beyond the mixed layer top: up to 30% of the surface momentum flux is still present in the cloud layer ($z/z_i = 1.3$).

Whether the clouds themselves, by triggering larger or more effective momentum transport, lead to weaker surface wind shear cannot be answered without a detailed budget study that samples the momentum tendencies introduced by convective and cloudy plumes and by small-scale turbulence in LES, or by spectral analysis of the scales that contribute to the total momentum flux in observations and LES. A recent study using large-domain LES hindcasts of sub-tropical shallow convection reveal that dry convective plumes present within the mixed layer carry significant flux that tend to accelerate

near-surface winds (Helfer, Dixit and Nuijens, submitted). Dixit et al 2021 also show that horizontal transport in these simulations, presumably through mesoscale circulations that can develop in these open-boundary nested LES domains, drive larger momentum fluxes than found in traditional LES with cyclic boundary conditions. A spectral decomposition of momentum fluxes by eddy sizes derived from LES of organized shallow convection in a cold air outbreak demonstrates that larger eddies are accompanied by a momentum flux profile that can maximize in the mixed layer and accelerate near-surface winds (Saggiorato et al., 2020). Similar budget studies and spectral decomposition of the momentum fluxes are underway for Cabauw. We suspect that mesoscales are important in the real world, but not adequately captured in 10 min averaged eddy-covariance flux data or small LES domains with cyclic boundary conditions.

Acronyms

ATEX Atlantic Tradewind EXperiment
BOMEX Barbados Oceano-graphic and Meteorological Experiment
CC cloud cover (temporal)
cbh cloud base height
CLCC Clear-sky and cumulus regimes with limited cloud cover
DALES Dutch Atmospheric Large Eddy Simulation
ECMWF European Centre for Medium-Range Weather Forecasts
ERA5 ECMWF ReAnalysis version 5
GRASP GPU-resident Atmospheric Simulation Platform
LES Large Eddy Simulation
LCL Lifting Condensation Level
LLJ Low Level Jet
LWP Liquid Water Path
MOST Monin-Obukhov Similarity Theory
NWP Numerical Weather Prediction
RICO Rain in shallow Cumulus over the Ocean

Acknowledgments

This project has received funding from the European Research Council (ERC) under the European Union's Horizon 2020 research and innovation program (Starting Grant Agreement 714918). The measured data at Cabauw, along with the processing scripts are available from this site ([still needs to be made]).

References

Arrillaga, J. A., Vilà-Guerau de Arellano, J., Bosveld, F., Klein Baltink, H., Yagüe, C., Sastre, M., & Román-Cascón, C. (2018). Impacts of afternoon and evening sea-breeze fronts on local turbulence, and on co2 and radon-222 transport. *Quarterly Journal of the Royal Meteorological Society*, *144*(713), 990-1011. Retrieved from `https://rmets.onlinelibrary.wiley.com/doi/abs/10.1002/qj.3252` doi: 10.1002/qj.3252

Baas, P., Bosveld, F. C., Klein Baltink, H., & Holtslag, A. A. M. (2009, 08). A Climatology of Nocturnal Low-Level Jets at Cabauw. *Journal of Applied Meteorology and Climatology*, *48*(8), 1627-1642. Retrieved from `https://doi.org/10.1175/2009JAMC1965.1` doi: 10.1175/2009JAMC1965.1

Bolton, D. (1980, 07). The Computation of Equivalent Potential Temperature. *Monthly Weather Review*, *108*(7), 1046-1053. Retrieved from

https://doi.org/10.1175/1520-0493(1980)108<1046:TCOEPT>2.0.CO;2 doi: 10.1175/1520-0493(1980)108⟨1046:TCOEPT⟩2.0.CO;2

Bosveld, F. (1999). *The knmi gardren experiment: micro-metrological observations 1988 – 1989 corrections* (Vol. WR 99 - 03; Tech. Rep.). KNMI. Available athttp://bibliotheek.knmi.nl/knmipubWR/WR99-03.pdf(2020/08/26).

Bosveld, F. (2020). *The cabauw in-situ observational program 2000 – present: Instruments, calibrations and set-up* (Tech. Rep.). KNMI. Available athttp://projects.knmi.nl/cabauw/insitu/observations/documentation/Cabauw_TR/Cabauw_TR.pdf(2020/08/26).

Bosveld, F., Baas, P., Beljaars, A., Holtslag, A., Vil'a-Gerau de Arellano, J., & van de Wiel, B. (2020). Fifty years of atmospheric boundary-layer research at cabauw serving weather, air quality and climate. *Boundary-Layer Meteorology*. Retrieved from https://doi.org/10.1007/s10546-020-00541-w doi: 10.1007/s10546-020-00541-w

Bretherton, C. S., & Blossey, P. N. (2017). Understanding mesoscale aggregation of shallow cumulus convection using large-eddy simulation. *Journal of Advances in Modeling Earth Systems*, *9*(8), 2798-2821. Retrieved from https://agupubs.onlinelibrary.wiley.com/doi/abs/10.1002/2017MS000981 doi: 10.1002/2017MS000981

Brown, A. (1999). Large-eddy simulation and parametrization of the effects of shear on shallow cumulus convection. *Boundary-Layer Meteorology*, *91*, 65-80. Retrieved from https://doi.org/10.1023/A:1001836612775 doi: 10.1023/A:1001836612775

ECMWF. (2015). *Ifs documentation cy41r1.* Shinfield Park, Reading, RG2 9AX, England: Author. Retrieved from https://www.ecmwf.int/node/9211 (Operational implementation 12 May 2015) doi: 10.21957/p50qmwprw

Fodor, K., Mellado, J. P., & Wilczek, M. (2019). On the role of large-scale updrafts and downdrafts in deviations from monin–obukhov similarity theory in free convection. *Boundary-layer meteorology*, *172*(3), 371–396. Retrieved from https://link.springer.com/article/10.1007/s10546-019-00454-3

He, Y., Monahan, A. H., & McFarlane, N. A. (2013). Diurnal variations of land surface wind speed probability distributions under clear-sky and low-cloud conditions. *Geophysical Research Letters*, *40*(12), 3308–3314. doi: 10.1002/grl.50575

Heus, T., van Heerwaarden, C. C., Jonker, H. J. J., Pier Siebesma, A., Axelsen, S., van den Dries, K., ... Vilà-Guerau de Arellano, J. (2010). Formulation of the dutch atmospheric large-eddy simulation (dales) and overview of its applications. *Geoscientific Model Development*, *3*(2), 415–444. Retrieved from https://gmd.copernicus.org/articles/3/415/2010/ doi: 10.5194/gmd-3-415-2010

Holloway, C., Wing, A., & Bony, S. e. a. (2017). Observing Convective Aggregation. *Surv Geophys*, *38*, 1199–1236. Retrieved from https://doi.org/10.1007/s10712-017-9419-1 doi: 10.1007/s10712-017-9419-1

Jabouille, P., Redelsperger, J. L., & Lafore, J. P. (1996, 05). Modification of Surface Fluxes by Atmospheric Convection in the TOGA COARE Region. *Monthly Weather Review*, *124*(5), 816-837. Retrieved from https://doi.org/10.1175/1520-0493(1996)124<0816:MOSFBA>2.0.CO;2 doi: 10.1175/1520-0493(1996)124⟨0816:MOSFBA⟩2.0.CO;2

Lareau, N. P., Zhang, Y., & Klein, S. A. (2018). Observed boundary layer controls on shallow cumulus at the arm southern great plains site. *Journal of the Atmospheric Sciences*, *75*(7), 2235 - 2255. Retrieved from https://journals.ametsoc.org/view/journals/atsc/75/7/jas-d-17-0244.1.xml doi: 10.1175/JAS-D-17-0244.1

LeMone, M. A. (1983, 07). Momentum Transport by a Line of Cumulonimbus. *Journal of the Atmospheric Sciences*, *40*(7), 1815-1834. Retrieved from

https://doi.org/10.1175/1520-0469(1983)040<1815:MTBALO>2.0.CO;2 doi: 10.1175/1520-0469(1983)040⟨1815:MTBALO⟩2.0.CO;2

LeMone, M. A., & Jorgensen, D. P. (1990, 11). Precipitation and Kinematic Structure of an Oceanic Mesoscale Convective System. Part I: Momentum Transport and Generation. *Monthly Weather Review*, *119*(11), 2638-2653. Retrieved from https://doi.org/10.1175/1520-0493(1991)119<2638:PAKSOA>2.0.CO;2 doi: 10.1175/1520-0493(1991)119⟨2638:PAKSOA⟩2.0.CO;2

LeMone, M. A., & Pennell, W. T. (1976). The Relationship of Trade Wind Cumulus Distribution to Subcloud Layer Fluxes and Structure. *Monthly Weather Review*, *104*(5), 524–539. Retrieved from http://dx.doi.org/10.1175/1520-0493(1976)104{\%}3C0524:TROTWC{\%}3E2.0.CO{\%}5Cn2 doi: 10.1175/1520-0493(1976)104⟨0524:TROTWC⟩2.0.CO;2

Li, D., & Bou-Zeid, E. (2011, 4). Coherent Structures and the Dissimilarity of Turbulent Transport of Momentum and Scalars in the Unstable Atmospheric Surface Layer. *Boundary-Layer Meteorology*, *140*, 243-262. Retrieved from https://doi.org/10.1007/s10546-011-9613-5 doi: 10.1007/s10546-011-9613-5

Liu, S., Zeng, X., Dai, Y., & Shao, Y. (2019). Further improvement of surface flux estimation in the unstable surface layer based on large-eddy simulation data. *Journal of Geophysical Research: Atmospheres*, *124*(17-18), 9839-9854. Retrieved from https://agupubs.onlinelibrary.wiley.com/doi/abs/10.1029/2018JD030222 doi: 10.1029/2018JD030222

Moeng, C.-H., & Sullivan, P. P. (1994). A comparison of shear- and buoyancy-driven planetary boundary layer flows. *Journal of Atmospheric Sciences*, *51*(7), 999 - 1022. Retrieved from https://journals.ametsoc.org/view/journals/atsc/51/7/1520-0469_1994_051_0999_acosab_2_0_co_2.xml doi: 10.1175/1520-0469(1994)051⟨0999:ACOSAB⟩2.0.CO;2

Nuijens, L., Serikov, I., Hirsch, L., Lonitz, K., & Stevens, B. (2014). The distribution and variability of low-level cloud in the north atlantic trades. *Quarterly Journal of the Royal Meteorological Society*, *140*(684), 2364-2374. Retrieved from https://rmets.onlinelibrary.wiley.com/doi/abs/10.1002/qj.2307 doi: 10.1002/qj.2307

Romps, D. (2017, 09). Exact expression for the lifting condensation level. *Journal of the Atmospheric Sciences*, *74*. doi: 10.1175/JAS-D-17-0102.1

Rotunno, R., Klemp, J. B., & Weisman, M. L. (1988, 02). A Theory for Strong, Long-Lived Squall Lines. *Journal of the Atmospheric Sciences*, *45*(3), 463-485. Retrieved from https://doi.org/10.1175/1520-0469(1988)045<0463:ATFSLL>2.0.CO;2 doi: 10.1175/1520-0469(1988)045⟨0463:ATFSLL⟩2.0.CO;2

Saggiorato, B., Nuijens, L., Siebesma, A. P., de Roode, S., Sandu, I., & Papritz, L. (2020). The influence of convective momentum transport and vertical wind shear on the evolution of a cold air outbreak. *Journal of Advances in Modeling Earth Systems*, *12*(6), e2019MS001991. Retrieved from https://agupubs.onlinelibrary.wiley.com/doi/abs/10.1029/2019MS001991 (e2019MS001991 10.1029/2019MS001991) doi: 10.1029/2019MS001991

Schalkwijk, J., Bosveld, F. C., & Siebesma, A. P. (2010). *Timescales and structures in vertical transport in the atmospheric boundary layer.*

Schalkwijk, J., Jonker, H. J. J., Siebesma, A. P., & Bosveld, F. C. (2015, 02). A Year-Long Large-Eddy Simulation of the Weather over Cabauw: An Overview. *Monthly Weather Review*, *143*(3), 828-844. Retrieved from https://doi.org/10.1175/MWR-D-14-00293.1 doi: 10.1175/MWR-D-14-00293.1

Schlemmer, L., Bechtold, P., Sandu, I., & Ahlgrimm, M. (2017). Uncertainties related to the representation of momentum transport in shallow convection. *Journal of Advances in Modeling Earth Systems*, *9*(2), 1269-1291. Retrieved from https://agupubs.onlinelibrary.wiley.com/doi/abs/10.1002/2017MS000915 doi: 10.1002/2017MS000915

Stevens, B. (2007, 08). On the Growth of Layers of Non-precipitating Cumulus Convection. *Journal of the Atmospheric Sciences*, *64*(8), 2916-2931. Retrieved from https://doi.org/10.1175/JAS3983.1 doi: 10.1175/JAS3983.1

Stevens, B., Bony, S., Ament, F., Bigorre, S., Chazette, P., Crewell, S., ... Wirth, M. (2017, 09). Eurec4a: A field campaign to elucidate the couplings between clouds, convection and circulation. *Surveys in Geophysics*, *38*, 1529-1568. Retrieved from https://doi.org/10.1007/s10712-017-9428-0 doi: 10.1007/s10712-017-9428-0

Sullivan, P. P., McWilliams, J. C., & Moeng, C. A. (1994). A subgrid-scale model for large-eddy simulation of planetary boundary-layer flows. *Boundary Layer Meteorology*, *71*, 247-279. Retrieved from https://doi.org/10.1007/BF00713741

Tung, W.-W., & Yanai, M. (2002, 09). Convective Momentum Transport Observed during the TOGA COARE IOP. Part II: Case Studies. *Journal of the Atmospheric Sciences*, *59*(17), 2535-2549. Retrieved from https://doi.org/10.1175/1520-0469(2002)059<2535:CMTODT>2.0.CO;2 doi: 10.1175/1520-0469(2002)059⟨2535:CMTODT⟩2.0.CO;2

Van Stratum, B. J. H., de Arellano, J., van Heerwaarden, C. C., & Ouwersloot, H. G. (2014). Subcloud-Layer Feedbacks Driven by the Mass Flux of Shallow Cumulus Convection over Land. *Journal of the Atmospheric Sciences*, *71*(3), 881–895. doi: 10.1175/JAS-D-13-0192.1

Wu, X., & Yanai, M. (1994, 06). Effects of Vertical Wind Shear on the Cumulus Transport of Momentum: Observations and Parameterization. *Journal of the Atmospheric Sciences*, *51*(12), 1640-1660. Retrieved from https://doi.org/10.1175/1520-0469(1994)051<1640:EOVWSO>2.0.CO;2 doi: 10.1175/1520-0469(1994)051⟨1640:EOVWSO⟩2.0.CO;2

Zhang, Y., & Klein, S. A. (2013, 04). Factors controlling the vertical extent of fair-weather shallow cumulus clouds over land: Investigation of diurnal-cycle observations collected at the arm southern great plains site. *Journal of the Atmospheric Sciences*, *70*(4), 1297 - 1315. Retrieved from https://journals.ametsoc.org/view/journals/atsc/70/4/jas-d-12-0131.1.xml doi: 10.1175/JAS-D-12-0131.1

Zhu, P. (2015, 11). On the Mass-Flux Representation of Vertical Transport in Moist Convection. *Journal of the Atmospheric Sciences*, *72*(12), 4445-4468. Retrieved from https://doi.org/10.1175/JAS-D-14-0332.1 doi: 10.1175/JAS-D-14-0332.1

Figure 1.

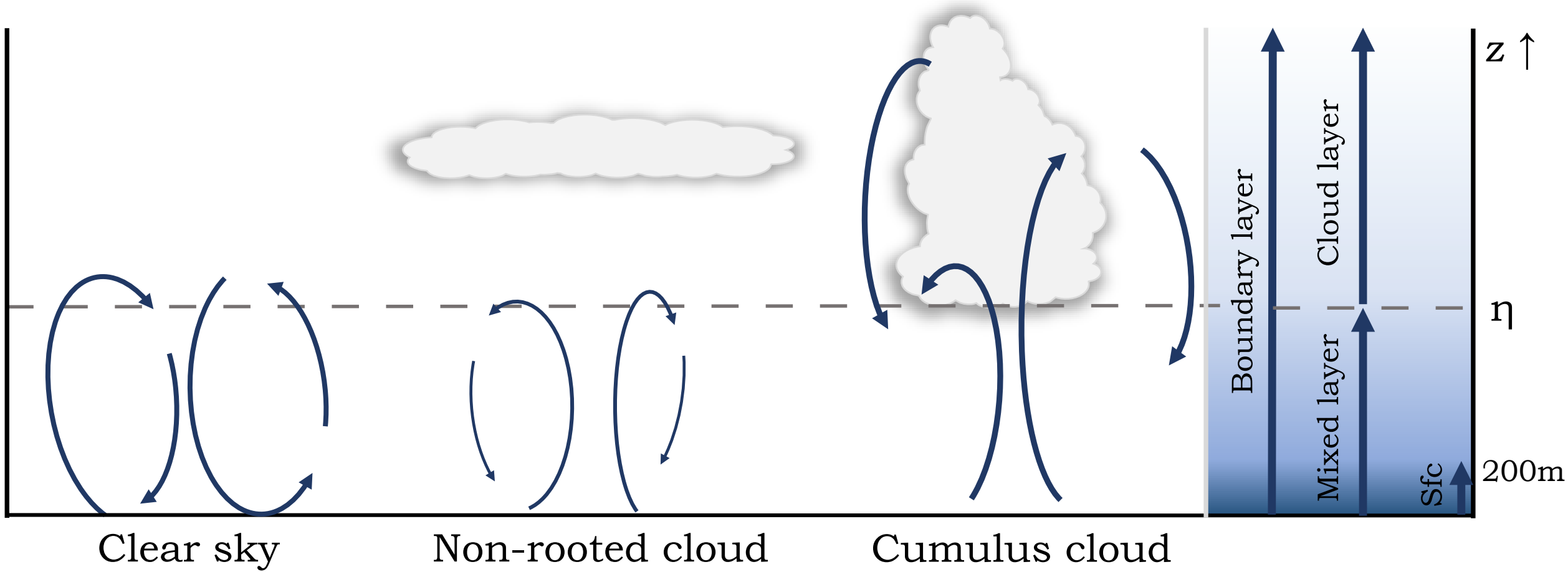
z
η
Boundary layer
Cloud layer
Mixed layer
Sfc
200m
Clear sky
Non-rooted cloud
Cumulus cloud

Figure 2.

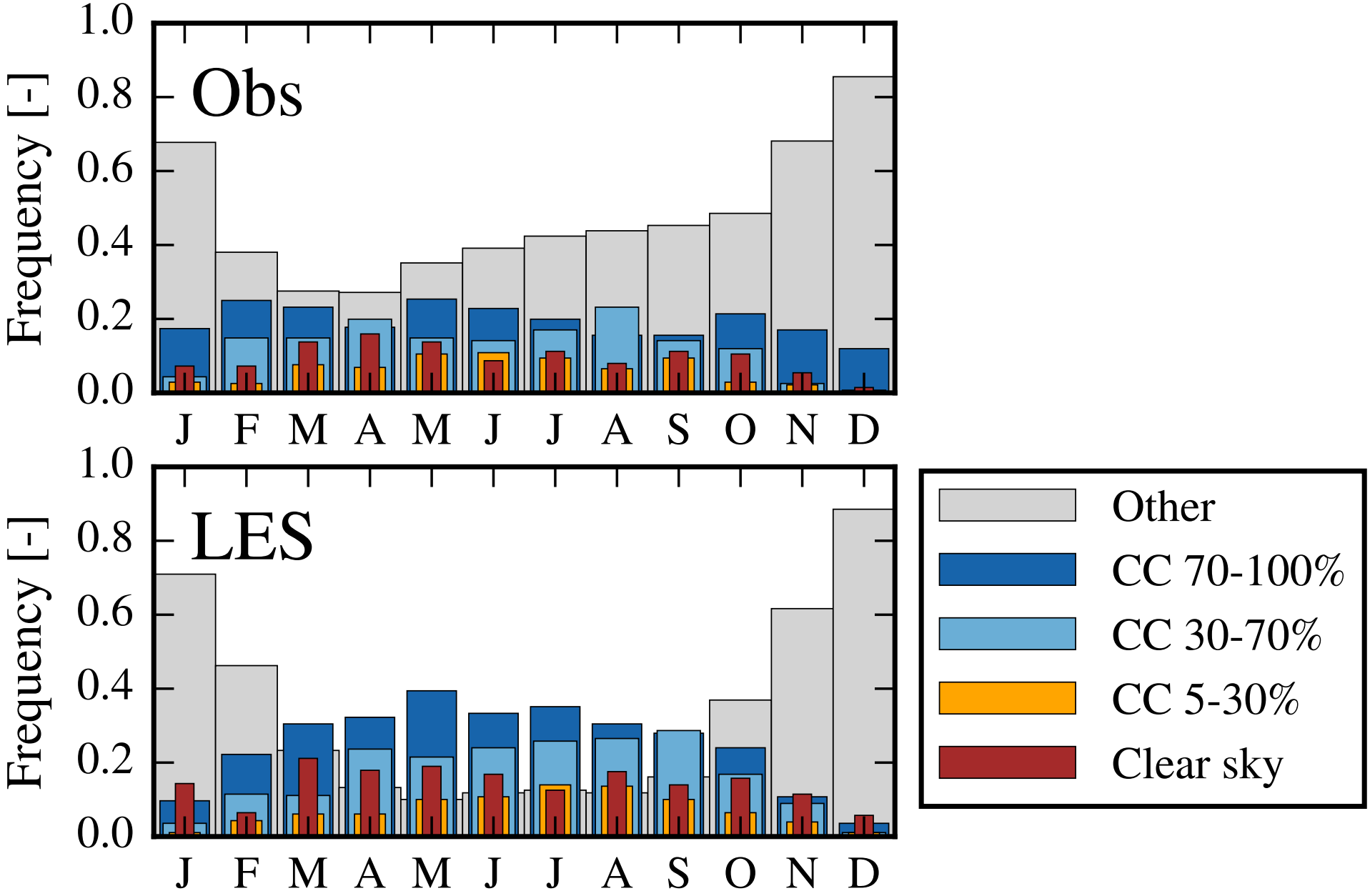
Obs
LES
Frequency [-]
1.0
0.8
0.6
0.4
0.2
0.0
J F M A M J J A S O N D
Other
CC 70-100%
CC 30-70%
CC 5-30%
Clear sky

Figure3.

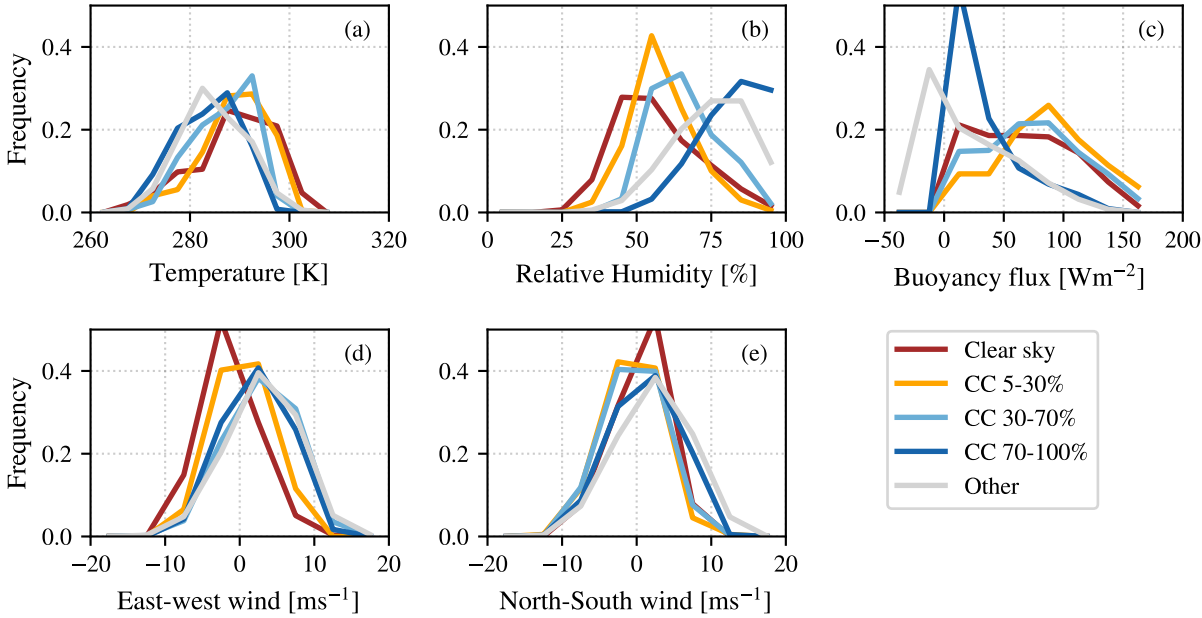
(a)
(b)
(c)
(d)
(e)
Frequency
Temperature [K]
Relative Humidity [%]
Buoyancy flux [Wm^{-2}]
East-west wind [ms^{-1}]
North-South wind [ms^{-1}]
Clear sky
CC 5-30%
CC 30-70%
CC 70-100%
Other

Figure 4.

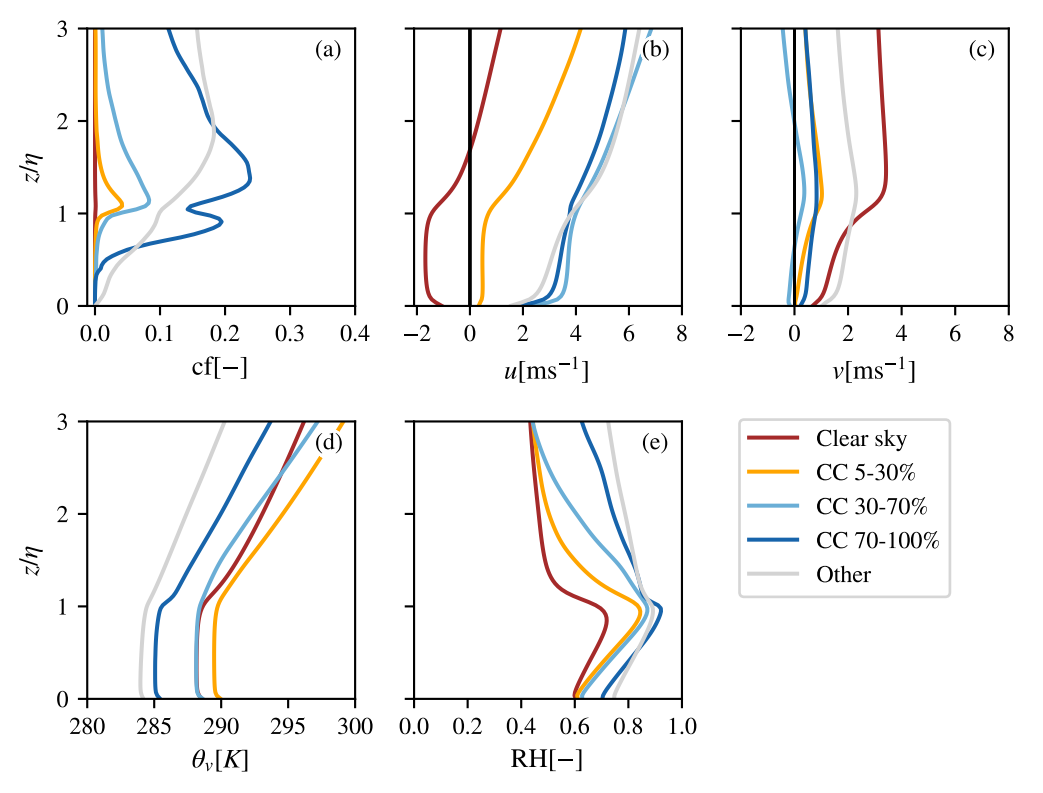
(a)
(b)
(c)
(d)
(e)
z/η
cf[−]
u[ms−1]
v[ms−1]
θv[K]
RH[−]
Clear sky
CC 5-30%
CC 30-70%
CC 70-100%
Other

Figure 5.

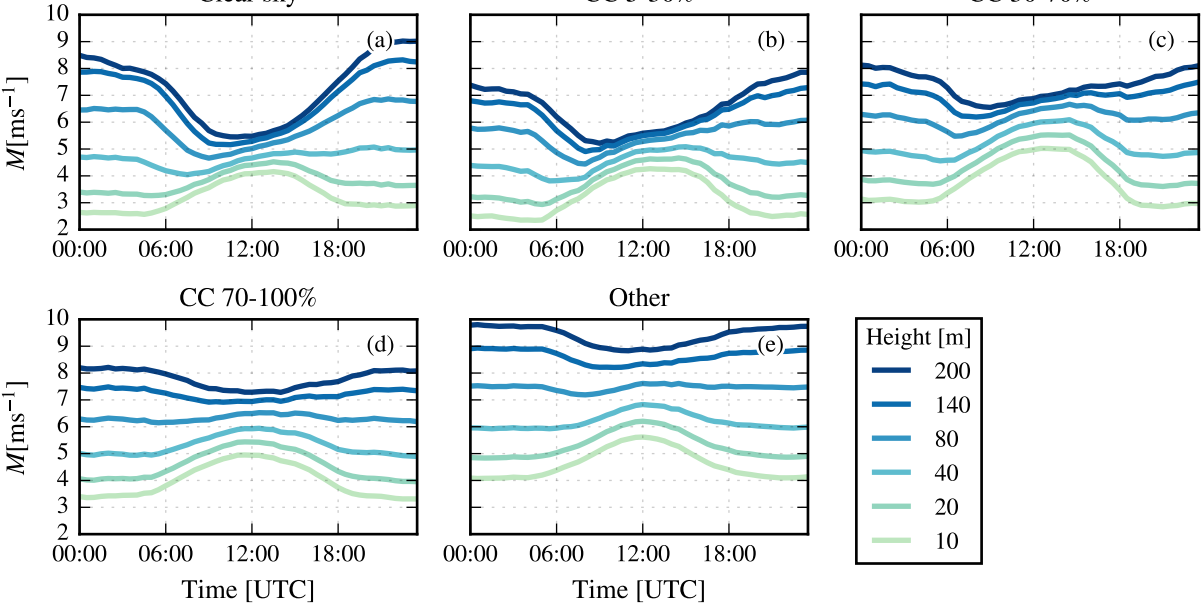
Clear sky
CC 5-30%
CC 30-70%
CC 70-100%
Other
(a)
(b)
(c)
(d)
(e)
M[ms−1]
10
9
8
7
6
5
4
3
2
00:00
06:00
12:00
18:00
Time [UTC]
Height [m]
200
140
80
40
20
10

Figure 6.

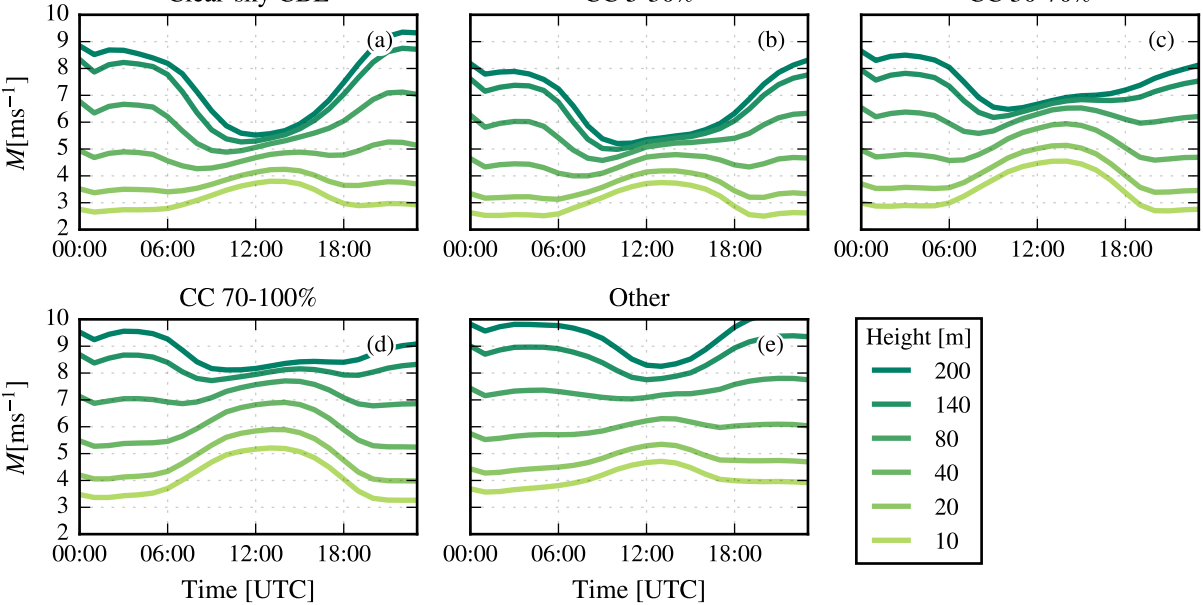
Clear-sky CBL
CC 5-30%
CC 30-70%
CC 70-100%
Other
(a)
(b)
(c)
(d)
(e)
M[ms−1]
10
9
8
7
6
5
4
3
2
00:00
06:00
12:00
18:00
Time [UTC]
Height [m]
200
140
80
40
20
10

Figure 7.

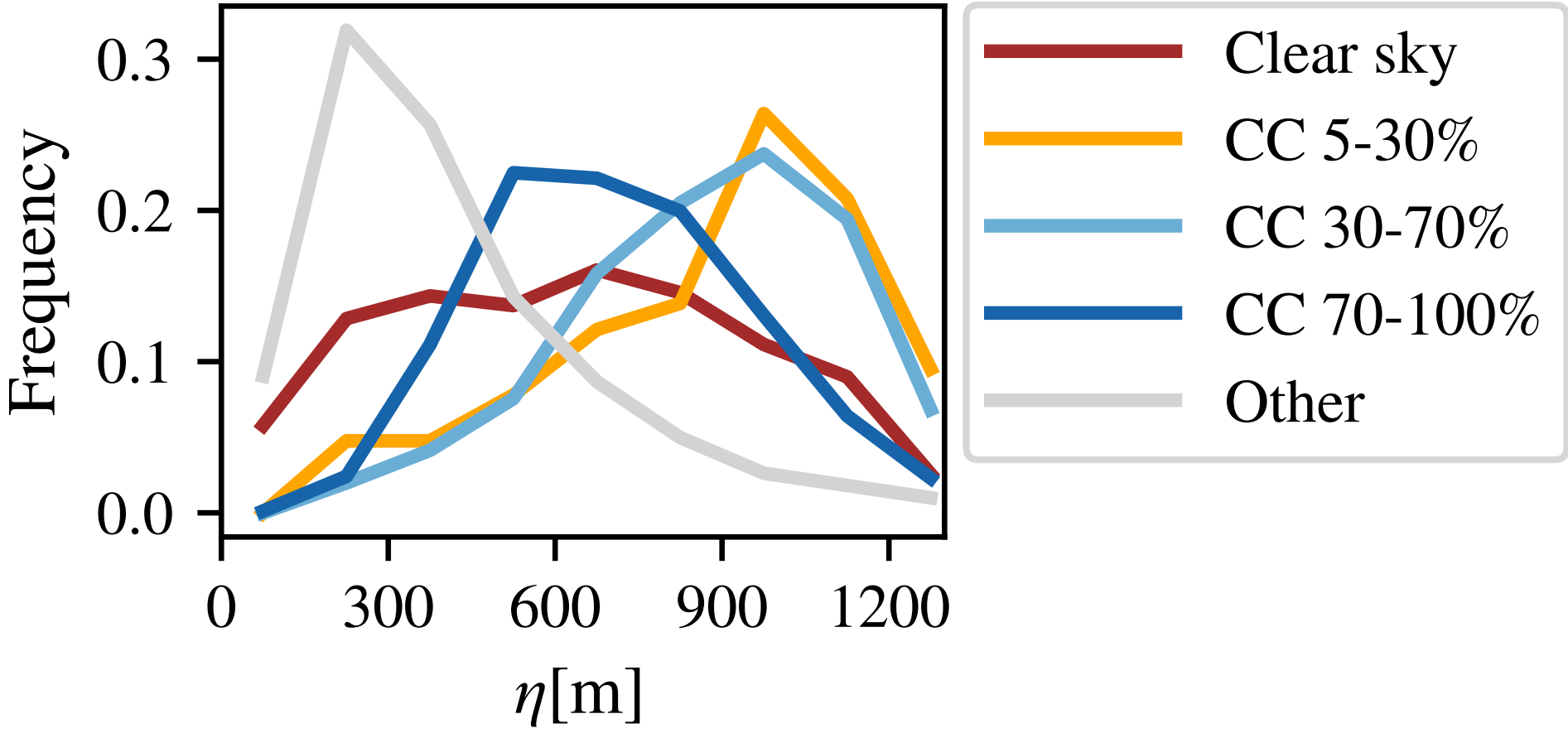
Frequency
0.3
0.2
0.1
0.0
0
300
600
900
1200
η[m]
Clear sky
CC 5-30%
CC 30-70%
CC 70-100%
Other

Figure 8.

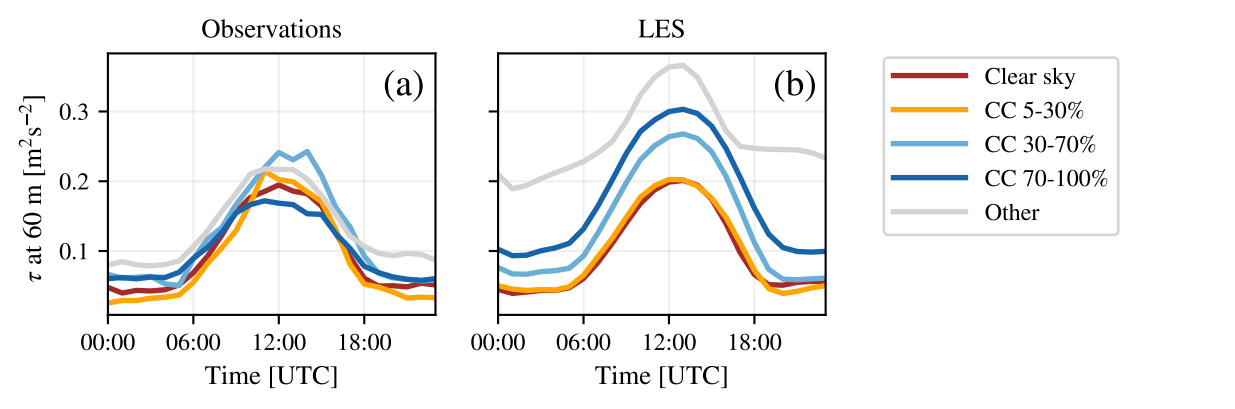
Observations
LES
(a)
(b)
τ at 60 m [$m^2 s^{-2}$]
0.3
0.2
0.1
00:00
06:00
12:00
18:00
Time [UTC]
Clear sky
CC 5-30%
CC 30-70%
CC 70-100%
Other

Figure 9.

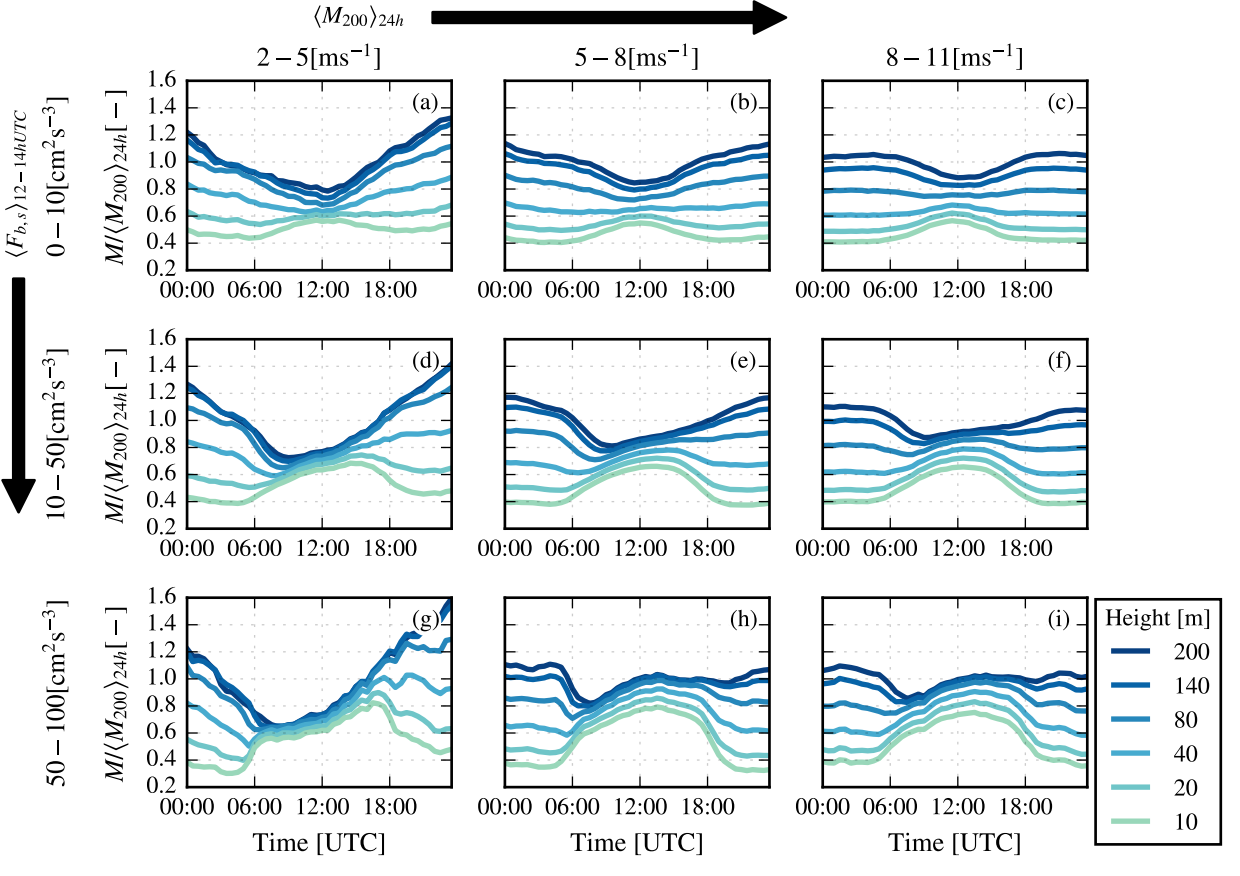
$\langle M_{200}\rangle_{24h}$
2 – 5[ms^{-1}]
5 – 8[ms^{-1}]
8 – 11[ms^{-1}]
$\langle F_{b,s}\rangle_{12-14hUTC}$
0 – 10[cm^{2}s^{-3}]
10 – 50[cm^{2}s^{-3}]
50 – 100[cm^{2}s^{-3}]
$M/\langle M_{200}\rangle_{24h}$[–]
(a)
(b)
(c)
(d)
(e)
(f)
(g)
(h)
(i)
00:00 06:00 12:00 18:00
Time [UTC]
Height [m]
200
140
80
40
20
10

Figure 10.

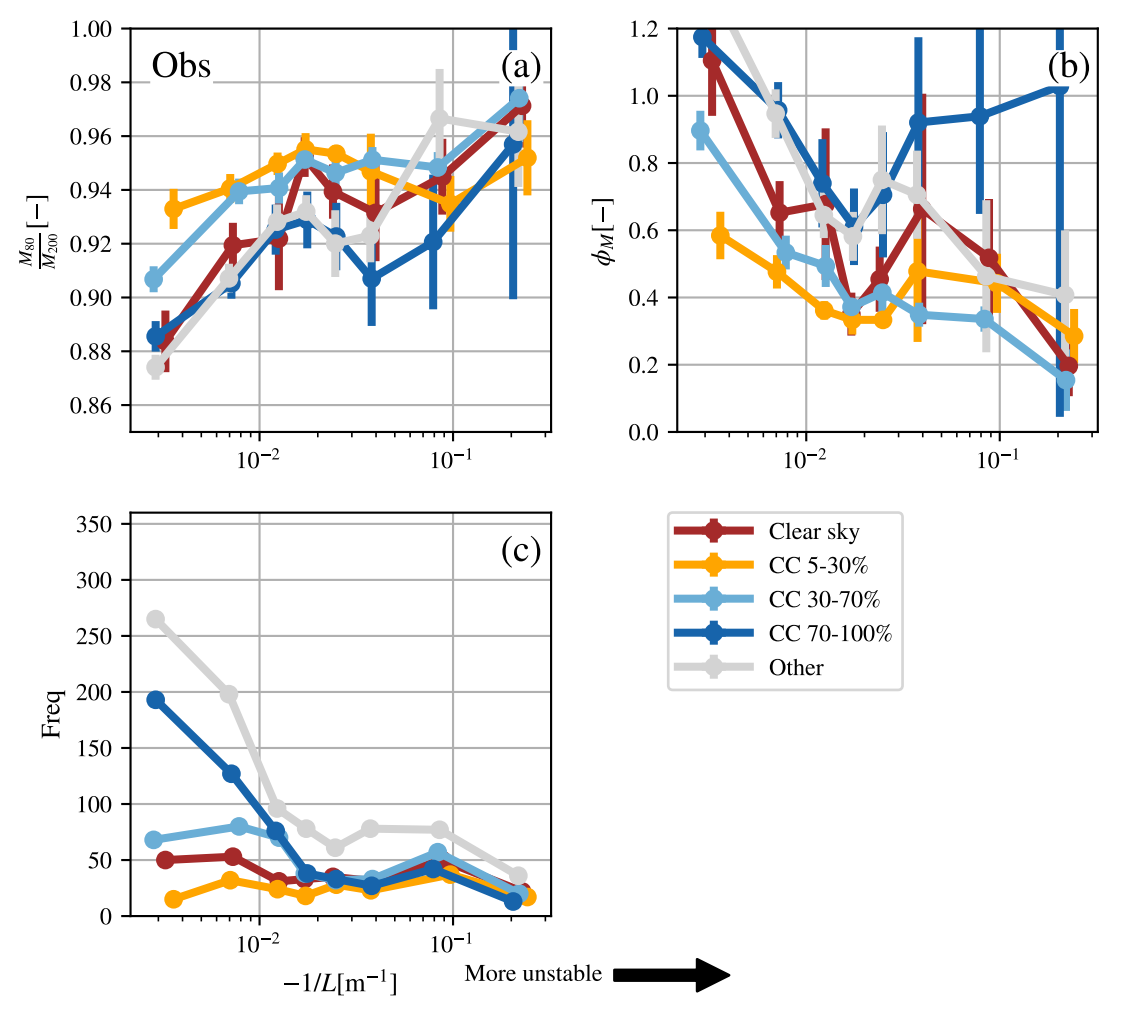
Obs
(a)
(b)
(c)
$\frac{M_{80}}{M_{200}}$ [−]
ϕ_M[−]
Freq
$-1/L$[m^{-1}]
More unstable
Clear sky
CC 5-30%
CC 30-70%
CC 70-100%
Other

Figure 11.

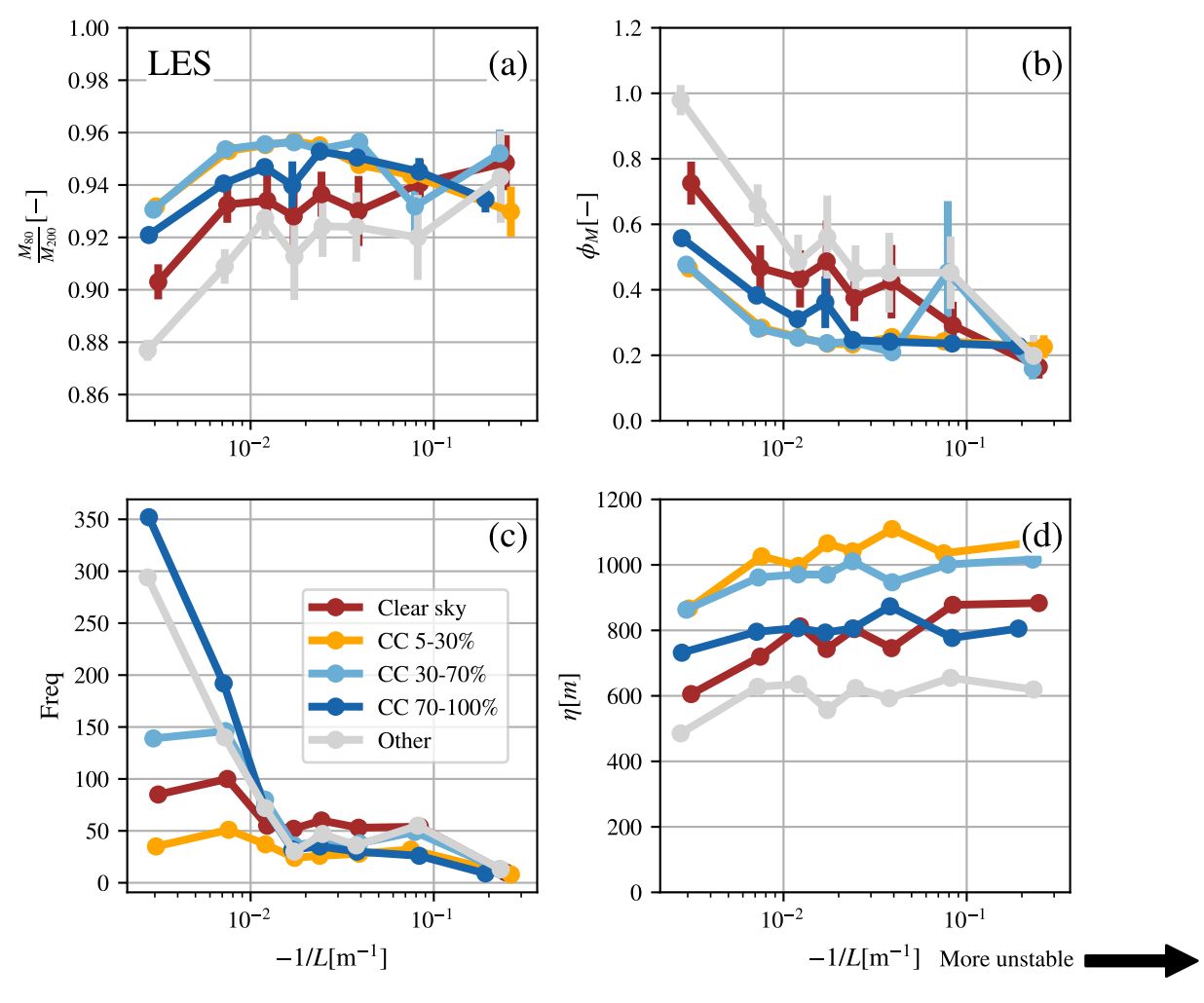
LES
(a)
(b)
(c)
(d)
$\frac{M_{80}}{M_{200}}$ [−]
ϕ_M[−]
Freq
$\eta[m]$
$-1/L[\mathrm{m}^{-1}]$
$-1/L[\mathrm{m}^{-1}]$ More unstable
Clear sky
CC 5-30%
CC 30-70%
CC 70-100%
Other

Figure 12.

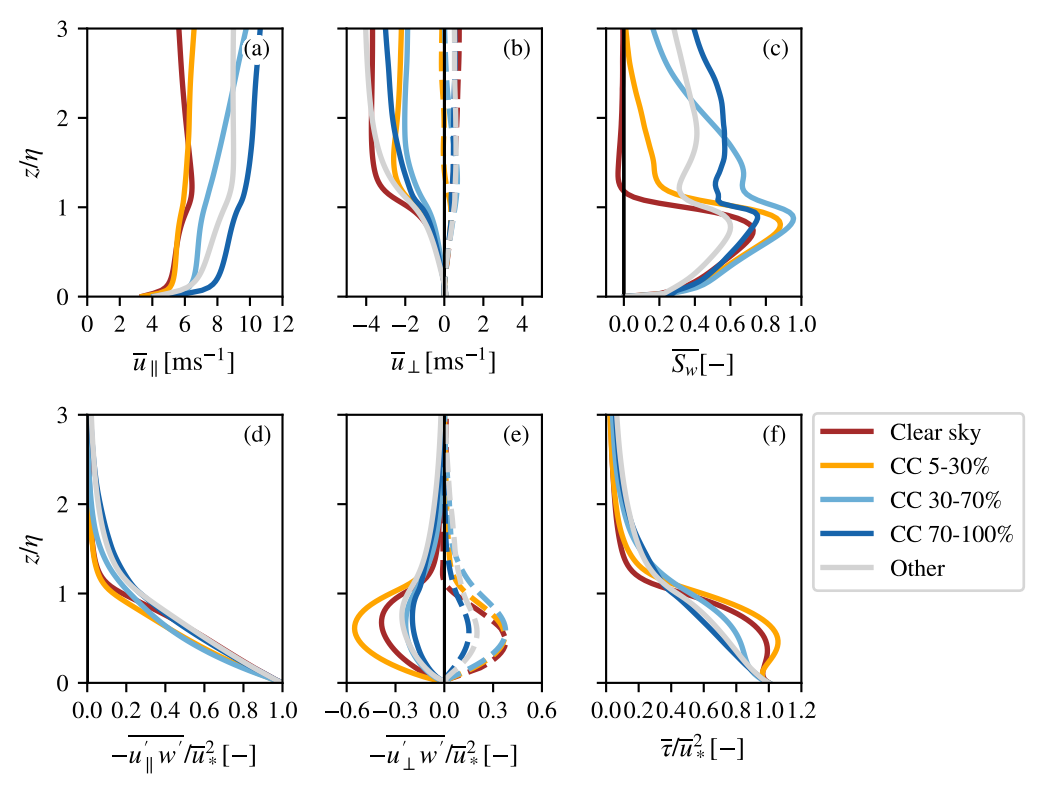
(a)
(b)
(c)
(d)
(e)
(f)
z/η
$\overline{u}_{\parallel}\,[\mathrm{ms}^{-1}]$
$\overline{u}_{\perp}\,[\mathrm{ms}^{-1}]$
$\overline{S_w}[-]$
$-\overline{u'_{\parallel}w'}/\overline{u}_*^2\,[-]$
$-\overline{u'_{\perp}w'}/\overline{u}_*^2\,[-]$
$\overline{\tau}/\overline{u}_*^2\,[-]$
Clear sky
CC 5-30%
CC 30-70%
CC 70-100%
Other